ORIGINAL ARTICLE

A pH/ROS dual-responsive system for effective chemoimmunotherapy against melanoma *via* remodeling tumor immune microenvironment

Leilei Wang[a], Shanshan He[a], Rong Liu[a], Yuan Xue[a], Yuan Quan[a], Rongying Shi[a], Xueying Yang[a], Qing Lin[a], Xun Sun[a], Zhirong Zhang[a], Ling Zhang[b,*]

[a]*Key Laboratory of Drug-Targeting and Drug Delivery System of the Education Ministry, West China School of Pharmacy, Sichuan University, Chengdu 610041, China*
[b]*Med-X Center for Materials, College of Polymer Science and Engineering, Sichuan University, Chengdu 610065, China*

Abstract Chemotherapeutics can induce immunogenic cell death (ICD) in tumor cells, offering new possibilities for cancer therapy. However, the efficiency of the immune response generated is insufficient due to the inhibitory nature of the tumor microenvironment (TME). Here, we developed a pH/reactive oxygen species (ROS) dual-response system to enhance chemoimmunotherapy for melanoma. The system productively accumulated in tumors by specific binding of phenylboronic acid (PBA) to sialic acids (SA). The nanoparticles (NPs) rapidly swelled and released quercetin (QUE) and doxorubicin (DOX) upon the stimulation of tumor microenvironment (TME). The *in vitro* and *in vivo* results consistently demonstrated that the NPs improved anti-tumor efficacy and prolonged survival of mice, significantly enhancing the effects of the combination. Our study revealed DOX was an ICD inducer, stimulating immune responses and promoting maturation of dendritic cells (DCs). Additionally, QUE served as a TME regulator by inhibiting the cyclooxygenase-2 (COX2)-prostaglandin E2 (PGE$_2$) axis, which influenced various immune cells, including increasing cytotoxic T cells (CLTs) infiltration, promoting M1 macrophage polarization, and reducing regulatory T cells (Tregs) infiltration. The combination synergistically facilitated chemoimmunotherapy efficacy by remodeling the immunosuppressive microenvironment. This work presents a promising strategy to increase anti-tumor efficiency of chemotherapeutic agents.

---

*Corresponding author.
  E-mail address: zhangling83@scu.edu.cn (Ling Zhang).

1. Introduction

Despite extensive research efforts, malignant tumors still pose a significant global health concern[1,2]. Common cancer treatments include surgical resection, chemotherapy, radiotherapy and biological therapy[3,4]. Among these options, chemotherapy remains the mainstay clinical therapy because of its simplicity and convenience[5,6]. Nevertheless, the non-specific selectivity and severe side effects of chemotherapeutic agents limit their effectiveness. In addition, tumor cells often exhibit marked resistance to a single chemotherapeutic agent[7−9]. To overcome these issues and improve anti-tumor efficiency, combination therapy has been shown to be an effective strategy[10,11]. Currently, as natural ingredients are increasingly explored and developed, their combination with other chemotherapeutic agents is also attractive[12,13].

Quercetin (QUE), a flavonol compound widely found in plants, is a highly sought-after natural substance[14−16]. QUE possesses a variety of pharmacological activities, such as anti-inflammatory, anti-tumor and antioxidant properties ect[17,18]. During recent years, the anti-cancer impact of QUE has been extensively investigated[19,20]. The mechanism associated with anti-cancer activity of QUE involves several signaling pathways, including apoptosis, PI3K/AKT, JAK/STAT, NF-KB, p53 and Wnt/β-catenin[19,20]. Wang et al.[21] prepared nanoparticles targeting delivery of QUE and found that it effectively reversed PTX resistance by inhibiting Akt and ERK phosphorylation and MMP depolarization. Similarly, some studies indicated that QUE enhanced the anti-cancer effects of drugs on cancer cells by downregulating the expression of drug efflux transporter proteins, p-glycoprotein (P-gp) and tumor resistance proteins[22]. However, previous combination studies have focused mainly on the impact of QUE on drug resistance or toxicity, neglecting its immunomodulatory role.

Cyclooxygenase-2 (COX2) plays a pivotal role in regulating the synthesis of prostaglandin E2 (PGE$_2$). PGE$_2$ inhibits cytotoxic T cells (CLTs) responses in the TME, including dendritic cells (DCs) antigen presentation and natural killer (NK) cells recruitment[23]. Furthermore, PGE$_2$ can recruit Tregs, further triggering immunosuppression[24−26]. As a result, high COX2 expression exacerbates immunosuppression in the tumor immune microenvironment (TME). Despite being little studied, QUE as a COX2 inhibitor may regulate the TME via the COX2-PGE$_2$ pathway[27,28]. While chemotherapeutic agents typically rely on potent cytotoxic effects to kill tumor cells, it has been found that anthracyclines such as DOX can induce immunogenic cell death (ICD)[29−31]. However, the immunogenicity induced by single tumor antigen-associated molecular patterns (DAMPs) is rather limited, highlighting the importance of improving the TME[16,32,33]. Consequently, combining an ICD inducer with a COX2 inhibitor would augment anti-tumor effects further. The poor aqueous solubility and low bioavailability of QUE severely limit its clinical utility[34]. Current studies are mostly confined to free drug or conventional delivery systems with low encapsulation rates[35−37]. Thus, it is imperative to develop a drug delivery system that can effectively deliver QUE/doxorubicin (DOX).

In this study, after confirming the combination effect of free DOX and QUE, we designed a dual-responsive tumor-targeting nano delivery system using a polymeric pre-drug micelle strategy with QUE pre-drug as a carrier. Firstly, the hydrophilic backbone dextran (DEX) was linked to phenylboronic acid (PBA) through reactive oxygen species (ROS)-responsive boronic acid ester bonding, yielding the polymer dextran-phenylboronic acid (DEX-PBA). Next, QUE was grafted onto DEX-PBA via acid-responsive ester bonding to obtain the polymer dextran-phenylboronic acid-quercetin (DEX-PBA-QUE). The DPQ-DOX nanoparticles (NPs) were then prepared by encapsulating DOX with DEX-PBA-QUE. The NPs are targeted to the tumor site by specific binding of PBA to sialic acid (SA), which is highly expressed at the tumor site. DOX and QUE can be rapidly released in response to the weak acid and ROS stimulation in TME. The introduction of QUE into the carrier via grafting improved the solubility of QUE and greatly enhanced QUE loading. We evaluated the in vitro responsiveness and cellular toxicity of DPQ-DOX NPs under varying pH and ROS situation. Moreover, we investigated the in vivo distribution and anti-tumor effects of DOX and QUE and explored their synergistic mechanism. DOX exerted its cytotoxicity against tumor cells, and the addition of QUE reduced tumor resistance by decreasing P-gp expression. Furthermore, DOX increased the tumor immunogenicity by induced ICD. QUE was a TME regulator that improved TME via inhibiting the COX2-PGE$_2$ axis. This combined strategy of ICD initiators and TME modulator enhanced immunity against tumor as evidenced by increased CTLs activation and decreased of immunoregulatory cells, such as higher proportions of mature DCs, NK cells, CD4$^+$ T cells and CD8$^+$ T cells, and lower proportions of CD4$^+$Foxp3$^+$CD25$^+$ T cells. Overall, compared to single agent or conventional co-loaded delivery systems, the DPQ-DOX NPs achieved an effective combination of chemotherapy and immunotherapy with better immune-enhancing effects, significant melanoma suppression and prolonged survival.

2. Materials and methods

2.1. Materials and animals

Six−eight weeks old male C57 mice and were obtained from Chengdu Dashuo Laboratory Animal Co., Ltd. All animal experiments were authorized by the Animal Ethics Committee of Sichuan University and conducted under the experimental guidelines of the Animal Experimentation Ethics Committee of Sichuan University. RAW 264.7 and B16F10 (mouse melanoma cell line) cells were cultured in Dulbecco's modified Eagles medium (DMEM, Gibco, Carlsbad, CA, USA) containing 10% fetal bovine serum and 5% streptomycin/penicillin at 37 °C in 5% CO$_2$ humidified environment.

2.2. Cytotoxicity of free DOX and QUE in vitro

The cytotoxicity of the combination of free DOX and QUE on B16F10 cells was evaluated by the 3-(4,5-dimethylthiazol-2)-2,5-diphenyltetrazolium bromide (MTT) method[38]. B16F10 cells were inoculated into 96-well plates at a concentration of 5×10^3 cells

each well and cultured for 24 h. After incubation, different concentrations of free DOX or QUE were added in per well, and cultured for a further 24 h. The culture solution was abandoned, 100 μL of MTT solution (1 mg/mL) was added and after 4 h of culture, the medium solution was carefully aspirated and the cells were lysed with 150 μL dimethyl sulfoxide (DMSO). The cells were shaken for 15 min (37 °C) in a thermostatic benchtop shaker and the absorbance was measured at 490 nm using a microplate reader (Varioskan Flash, Thermo Fisher Scientific, Waltham, MA, USA). In addition, the same MTT method was performed to measure the drug combination index (CI). The drug administration groups were in different concentrations of DOX, QUE and different ratios of the two drugs in combination (DOX/QUE, 4/1, 2/1, 1/1 and 1/2, m/m). The rest operations were completely same as the above. The CI was calculated as following Eq. (1):

$$CI = D_A/IC_{X,A} + D_B/IC_{X,B} \qquad (1)$$

where A and B represent two different drugs; $IC_{X,A}$ and $IC_{X,B}$ are the drug concentrations when the two drugs are used alone and the growth inhibition rate is X; D_A and D_B are the concentrations of the two drugs when the two drugs are used in combination and the growth inhibition rate is X.

2.3. Influence of DOX combined with QUE on cell apoptosis

The apoptosis of B16F10 cells induced by QUE, DOX or the combination of both was quantified using the Annexin V-FITC/PI Apoptosis Detection Kit (Shanghai Besai Biotechnology Co., Ltd.). Cells were inoculated into 6-well plates and cultured for 24 h. Cells were treated with DOX (312.5 ng/mL), QUE (3.2 μg/mL), DOX + QUE (312.5 ng/mL, 3.2 μg/mL) for 24 h, digested with trypsin and then resuspended in 1 × antibody binding buffer (PBS containing 2% FBS), according to the kit instructions, stain, gently mixed and incubated at 25 °C in an environment protected from light. After treatment, the cell status was detected by flow cytometry.

2.4. Determination of COX2 expression by Western blot experiment

The COX2 expression level was assessed by Western blot experiment. B16F10 cells and RAW cells were inoculated into 6-well plates and cultured overnight, while the cells were stimulated by the addition of 100 ng/mL lipopolysaccharide (LPS) and treated with different doses (0, 2.5, 5, 10, 20, 40 μmol/L) of QUE for 24 h. After diluted to a proper concentration, protein was quantified by BCA method (BCA kit, Solarbio, Beijing, China), loading buffer was added, protein was boiled for 10 min, and protein expression was detected according to the protein blotting procedure. For the *in vivo* assay, tumors from mice with different treatment were extracted, and subsequently lysed using a cell lysis buffer. The expression of COX2 was then assessed.

2.5. Synthesis and characterization of DEX-PBA-QUE

Activation of phenylboronic acid ester (to obtain CDI-PBA): 7.37 g of 4-hydroxyphenylboronic acid pinacol ester (PBA) and 10.2 g of carbonyl diimidazole (1,1'-carbonyldiimidazole, CDI) were dissolved in 46 mL of anhydrous dichloromethane and stirred for 30 min at 27 °C. Then 200 mL of ethyl acetate was added to the reaction solution, washed with H_2O (3 × 10 mL) to

remove unreacted CDI, washed once with saturated saline, dried over absolute sodium sulfate, filtered, evaporated to obtain CDI-PBA[39].

Synthesis of dextran-phenylboronic acid ester: 90 mg of dextran (Mw = 10,000 Da) and 150 mg of 4-dimethylaminopyridine (DMAP), 400 mg of CDI-PBA were completely dissolved in 5 mL of anhydrous DMSO and shaken overnight (37 °C, 100 rpm). After the reaction, an appropriate amount of ultrapure water was added to the reactive solution to precipitate the product, and after sufficient precipitation, the product was centrifuged at 8000 rpm (Sichuan Shuke Instrument Co., Ltd., Chengdu, China) for 15 min and washed with water three times. Finally, the precipitate was divided into beakers, pre-frozen at −40 °C and then lyophilized to obtain DEX-PBA[39,40].

Synthesis of DEX-PBA-QUE (for grafting QUE): 360 mg of DEX-PBA was weighed and dissolved in 5 mL of H_2O in a round bottom flask, 150 mg of QUE was dissolved in 10 mL of tetrahydrofuran and added dropwise to the solution of DEX-PBA and the reaction was lasted 10 h. The product solution was then spun off to remove THF. It was then added to a dialysis bag with a cut-off 1000 MW and lyophilized to obtain DEX-PBA-QUE, which was further confirmed by ^{1}H NMR and infrared spectroscopy.

2.6. Preparation and characterization of nanoparticles

Preparation of blank carrier nanoparticles by self-assembly utilizing the amphiphilic nature of the material[41]. The blank nanoparticles were diluted with PBS (pH 7.4), PBS (pH 6.5), PBS containing 1 mmol/L H_2O_2 (pH 7.4), PBS containing 1 mmol/L H_2O_2 (pH 6.5) at a ratio of 1:4 (v/v), respectively, and then 200 μL was incorporated into a 96-well plate, and the absorbance changes were measured continuously at 550 nm using a microplate reader (Varioskan Flash, Thermo Fisher Scientific, USA) at different time points. The degradation was calculated by Eq. (2):

$$Degradation\ (\%) = 100 \times (A - A_\infty)/(A_0 - A_\infty) \qquad (2)$$

where A is the absorbance, A_0 is the initial absorbance and A_∞ is the absorbance after complete degradation[39].

We prepared the drug-loaded nanoparticles with reference to the method of w/o/w emulsion and solvent volatilization[42]. Briefly, 20 mg of DEX-PBA-QUE was dispersed in THF with an appropriate dose of DOX. The mixture was sonicated for 3 min at 120 w; and then hydrated with PBS and sonicated for a further 6 min at 180 w. The THF was ultimately removed by spin evaporation to obtain drug-loaded nanoparticles. In the same way, the DP-DOX NPs were prepared by encapsulating DOX with DEX-PBA; blank nanoparticles DPQ NPs were prepared with carrier materials for subsequent experiments. To characterize the nanoparticles, a Zetasizer Nano ZS90 (Malvern Instruments, UK) was utilized to measure the size and zeta potential of DPQ-NP DOX nanoparticles. The morphology and size distribution were observed by transmission electron microscopy (TEM, Hitachi H-600, Japan). The nanoparticles were dispersed in PBS (pH 6.5) for 24 h and 1 mmol/L H_2O_2 pH 7.4 PBS for 4 h, respectively, and the changes in nanoparticle morphology were observed by TEM. The stabilities of DPQ-DOX NPs were investigated in PBS (pH 7.4, 25 °C) and DMEM medium (containing 10% FBS, 37 °C) *via* testing their hydrodynamic diameters at fixed time points. Classical gel chromatography (GC) was chosen to remove free DOX, and QUE and DOX were quantified by high performance liquid

chromatography (HPLC) to determine the encapsulation rate and drug loading capacity of the nanoparticles.

2.7. In vitro release experiment of DPQ-DOX NPs

The *in vitro* release research was carried out under sink conditions using dialysis. To detect drug release, the release medium was pH 7.4 PBS, pH 6.5 PBS, pH 7.4 PBS with 1 mmol/L H_2O_2, pH 6.5 PBS with 1 mmol/L H_2O_2. Free DOX and QUE, DPQ-DOX NPs were placed in 3000 kDa MWCO dialysis bags and immersed in release medium mentioned above and shaken gently (100 rpm) in a shaker at 37 °C for 72 h. At the indicated time, 1 mL of release medium was aspirated and replaced with 1 mL of fresh release medium. The concentrations of DOX were measured by fluorescence spectrophotometer after dilution with solvent.

2.8. Cellular uptake of the DPQ-DOX NPs

B16F10 cells were seeded in confocal dishes, incubated overnight at 37 °C and treated with free DOX, DP-DOX NPs and DPQ-DOX NPs at a concentration of 10 ng/mL DOX. After 2 h incubation, the cells were washed with pre-cooled PBS, fixed in 4% paraformaldehyde for 15 min and stained with 4′,6-diamidino-2-phenylindole (DAPI). Then the cells photographs were taken with a laser scanning confocal microscope (CLSM, Nikon, Chiyoda-ku, Tokyo, Japan). In addition, flow quantification was performed to determine whether PBA can promote cellular uptake of DOX. B16F10 cells were inoculated into 24-well plates and cultivated overnight. Free DOX, DP-DOX NPs, DPQ-DOX NPs were diluted to 400 ng/mL with media and then addition to cells. After incubation of 2 h, the cells were rinsed twice with pre-chilled PBS, digested with trypsin and finally resuspended with 0.4 mL of PBS. Finally, the mean fluorescence intensity was assessed by flow cytometry (Cytomics™ FC 500, Beckman Coulter, Miami, FL, USA). To further determine whether DPQ-DOX NPs enhanced uptake of DOX, LC−MS/MS was used. After uptake treatment, cells were rinsed and digested as described above, then resuspended in 200 μL ddH$_2$O and repeatedly freeze-thawed 4−5 times in liquid nitrogen. The intracellular DOX contents were analyzed visa liquid chromatography-tandem mass spectrometry (LC−MS/MS, Agilent 6410B, USA). The uptake inhibition assay was performed by adding the inhibitor PBA/SA to evaluate the binding of PBA to SA *in vitro*[43]. B16F10 cells were incubated with PBS or 5 mmol/L 3-aminobenzeneboronic acid (APBA)/SA for 1 h after overnight inoculation. Then, different groups of cells were treated with the same concentration of DPQ-DOX NPs. The rest of experiments were performed in the same way as the previous uptake assays. Similarly, the uptake of nanoparticles by B16F10 cells was determined by CLSM or flow cytometry.

2.9. Tumor model

Male C57 BL/6 mice were subcutaneously inoculated with B16F10 cells (1×10^5 cells/mice) on the right side to establish a B16F10 melanoma bearing mouse model. Tumor volume (mm^3) was recorded daily as in Eq. (3):

$$\text{Tumor volume} = (\text{Length}-\text{Width}^2)/2 \qquad (3)$$

where length is the length of the tumor, width is the short diameter of the tumor.

2.10. In vivo distribution experiments

To observe the tumor targeting of DPQ NPs *in vivo*, B16F10 tumor-bearing mice with 200−400 mm^3 tumor volume were randomly divided into four groups and administered with sterile saline, DiD, DP-DiD NPs, DPQ-DiD NPs at a dose of 200 μg/kg. After 2, 4, 8 and 12 h of intravenous injection, the mice were ethically executed and imaged using the IVIS spectrum system. To observe the distribution in the tumor tissue, tumor tissues from mice executed at 8 h were collected, fixed with optimal cutting temperature compound (OCT) and frozen at −80 °C. The samples were then cut into thin sections using a freezing microtome, stained and imaged by CLSM to observe the distribution of DiD. To further quantify the distribution of DOX in tumor-bearing mice, the distribution experiment was also conducted using DPQ-DOX NPs. Tumor-bearing mice were randomized into four groups and then intravenously injected with sterile saline, free DOX, DP-DOX NPs and DPQ-DOX NPs at a dosage of 5 mg/kg. The mice were executed and organs were collected at the time of sampling. The organs were homogenized by adding twice the volume of saline through a homogenizer (Precellys 24, Bertin, France). The distribution of DOX in each tissue was determined by LC−MS/MS.

2.11. Pharmacokinetics of DPQ-DOX NPs

Male Sprague−Dawley (SD) rats (200 ± 3 g) were used to explore the pharmacokinetics and 3 groups of rats were single i.v. injected with DOX, DP-DOX NPs, DPQ-DOX NPs at a dose of 5 mg/kg DOX. The blood samples were then taken from the mice at the fixed time point, centrifuged to get plasma, and the amount of DOX in plasma was measured by LC−MS/MS.

2.12. In vitro anti-tumor efficacy study

The cytotoxicity evaluation was still performed by MTT assay. B16F10 cells were inoculated into 96-well plates and incubated overnight in pH 7.4, pH 6.5, pH 7.4 with 1 mmol/L H_2O_2, pH 6.5 with 1 mmol/L H_2O_2 medium, respectively. Then free DOX, free QUE, DOX plus QUE, DP-DOX NPs, DPQ-DOX NPs with a gradient concentration (156, 312, 625, 1250, and 2500 ng/mL) were added to per well and treated for 24 h. The rest of the procedures were the same as before. Besides, RAW 264.7 was also treated with different concentrations of DPQ NPs. In the same way, the cytotoxicity of blank nanoparticles was detected by MTT. Similarly, the effect of free QUE, DOX, QUE plus DOX and DPQ-DOX NPs on apoptosis under different conditions was examined using the previous kits.

2.13. In vivo anti-tumor efficacy study

The tumor-bearing mice were randomly divided into 5 groups and intravenously administered with sterile saline, blank nanoparticles DPQ NPs, free DOX, DP-DOX NPs and DPQ-DOX NPs. The different formulations were given every 2 day at a dose of 3 mg/kg and the tumor volumes of the mice were recorded. Day 1 was defined as the treatment day for the first administration of the treated tumor-bearing mice. On Day 11, some of the mice were anesthetized and sacrificed. Tumors were collected, photographed and weighed. The tumor growth inhibition rate (TGI) was calculated as Eq. (4):

$$TGI (\%) = (1 - W_{treatment})/W_{control} \times 100 \qquad (4)$$

where $W_{treatment}$ and $W_{control}$ represent the mean tumor weight of the treated and control groups, respectively. Tumor tissues were embedded in paraffin and stained with hematoxylin and eosin (H&E), TUNEL and Ki 67 immunohistochemistry to evaluate the anti-tumor effects. The survival time of the remaining mice in different groups was recorded, monitored and analyzed.

2.14. In vitro DCs maturation

Bone marrow derived cells (BMDCs) were extracted and plated after incubation to Day 7 according to the literature method[44,45]. Then, the DCs were incubated for 24 h with the supernatant collected from B16F10 cell medium pre-treated with QUE, DOX, QUE + DOX, DP-DOX NPs, DPQ-DOX NPs. After 24 h incubation, the DCs were labeled with corresponding antibodies (anti-CD11C, anti-CD40, anti-CD80, anti-CD86) and the stained cells were measured by flow cytometry.

2.15. In vivo anti-tumor immune therapy effect study

To evaluate the anti-tumor immune therapy effect, B16F10 tumor-bearing mice were randomly divided into 8 groups, and intravenously administered with sterile saline, QUE, DOX, QUE + DOX, DPQ NPs, DP-DOX NPs, DP-DOX + QUE NPs and DPQ-DOX NPs, respectively. The administration schedule and dosage were the same as in the anti-tumor efficacy study mentioned above. After the completion of administration, the mice were anesthetized and sacrificed. Then the tumors, lymph nodes and spleens were collected and crushed, and the cells were pressed through 70 μm cell strainers for preparing single cell suspensions[46,47]. Some of the collected cells were labelled with CD11b, F4/80, CD86, and CD206 antibodies to analyze macrophages phenotypes. Some were labelled with CD3, CD8, CD4 and NK1.1 antibodies to identify T cells and NK cells. And some cells were stained with the antibodies mentioned in the previous in vitro assay antibodies to assess the maturation of DCs. These stained cells were examined by flow cytometry. Randomly selected tumor tissues were paraffin embedded and immunohistochemistry/immunofluorescence was performed to detect the expression of COX2, calreticulin (CRT), high mobility group protein B1(HMGB1), P-gp and C−C motif chemokine receptor 7 (CCR7). The expression level of COX2 in tumor tissues was also determined by Western blot. ELISA was used to assess the PGE_2 level in vivo and in vitro. Tumor tissues were collected, homogenized in PBS containing protease inhibitors, and centrifuged at 12,000 rpm (Anhui Zhongke Zhongjia scientific Instrument Co., Ltd., Hefei, China) for 10 min. The supernatant was collected for PGE_2 assay according to the kit instruction. B16F10 cells were seeded in the plate and treated with QUE, DOX, QUE + DOX, DP-DOX NPs, DPQ-DOX NPs, respectively. The medium was collected and the PGE_2 level in the supernatant was quantified using the PGE_2 kit.

2.16. Safe evaluation

To evaluate the toxicity of NPs, we monitored the body weights of the mice and sampled their blood on Day 11. The changes in WBC, RBC and PLT were measured using an automated hematology analyzer (MEK-6318K, Nijon-kohden, Shinjuku-ku, Japan). The enzyme activities of AST, ALT, LDH, CK, CREA and UA were measured by an automated biochemistry analyzer

(Hitachi). H&E staining was performed on major organs at the end of treatment.

2.17. Statistical analyses

All data were analyzed by GraphPad Prism software (GraphPad Software, Boston, MA, USA). Statistical significance was evaluated by one-way analysis of variance (ANOVA) with Tukey's multiple comparisons post hoc test and two-tailed Student's t-test. Statistical significance was defined as $^{*}P < 0.05$, $^{**}P < 0.01$, $^{***}P < 0.001$, and $^{****}P < 0.0001$.

3. Results and discussion

3.1. Cytotoxicity and synergistic effect of DOX and QUE on B16F10 cells

To ascertain whether QUE can enhance the toxicity of DOX on B16F10 cells, we measured the effect of various concentrations of DOX or QUE on B16F10 cells viability using the MTT assay. As shown in Fig. 1A and B, the low concentrations of QUE were almost non-cytotoxic or even promoted the growth of tumor cells. When the concentration reached 24 μmol/L, it exhibited a slight toxicity and the cell survival rate was more than 80%.QUE in combination with a low dose of DOX (156 ng/mL) increased the cytotoxicity, and the toxicity became stronger as the concentration of QUE increased. The cell viability rate decreased from $87.09 \pm 1.45\%$ to $50.45 \pm 3.05\%$ (Fig. 1B). Similarly, except at extremely small doses (78 ng/mL), DOX is more cytotoxic than alone when combined with QUE (1 μmol/L), the IC_{50} of DOX for B16F10 cells decreased from 1388 ng/mL to 664.8 ng/mL (Fig. 1C). Apoptosis reagent was then used to analysis the apoptosis of B16F10 after various drug treatments. The apoptosis rate was $6.71 \pm 0.48\%$ and $26.46 \pm 1.16\%$ after QUE or DOX alone, respectively, and increased to 37.6% after combined use, the IC_{50} of DOX plus QUE was half that of DOX alone (Fig. 1E and F). The above results indicated that the addition of QUE increased the cytotoxicity of DOX. We measured CI for exploring whether this effect was superimposed or synergistic. When the CI < 0.9, the drugs are synergistic in combination. The lower the CI, the stronger the synergy[48]. As shown in the results (Fig. 1D), the combination of DOX and QUE produced a synergistic effect on B16F10 cells and the synergistic effect was better when DOX/QUE (w/w) was 1.

Next, we focused on whether QUE affects the expression of COX2. The cells were first stimulated with LPS to mimic the in vivo environment, and then treated with different doses of QUE[49,50]. RAW264.7 cells stimulated with LPS (10 μg/mL) were selected as a positive control[51,52]. As shown in Fig. 1G, QUE significantly reduced COX2 expression in RAW264.7 cells even at low doses. In B16F10 cells, although there was almost no difference at low QUE concentration (2.5 μmol/L), the band of COX2 gradually weakened with increasing QUE concentration, which was further confirmed by image J analysis. When the QUE concentration was 40 μmol/L, the expression ratio of COX2 was $24.53 \pm 0.88\%$, which decreased the expression of COX2 by more than 4 times (Fig. 1H and I). Thus, QUE inhibited COX2 expression in RAW264.7 and B16F10 cells in a concentration-dependent manner. In general, the combination could increase the cellular toxicity of DOX and has the potential to inhibit the up-regulation of $COX2-PGE_2$ axis at the tumor site, but it may depend on high concentrations of QUE.
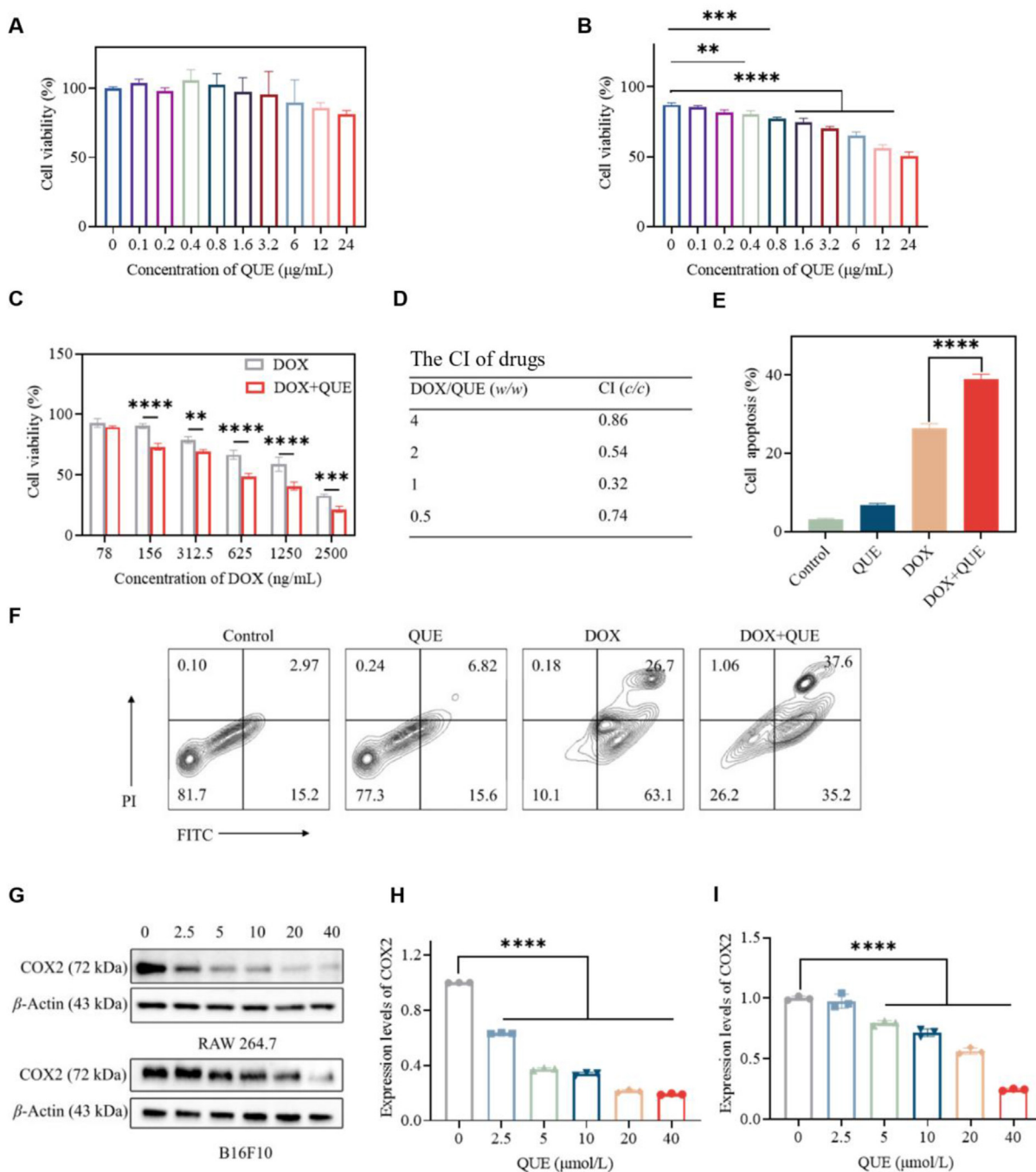
Figure 1 *In vitro* combination effect of DOX and QUE. (A−C) Cytotoxicity of varying concentrations of QUE (A), QUE with 156 ng/mL DOX (B) and DOX with 3.2 μg/mL QUE (C) on B16F10 cells was assessed. (D) The CI of DOX and QUE in different ratios. (E) The relative proportions of apoptosis induced by QUE or DOX. (F) Flow cytometry analysis of apoptotic B16F10 cells treated with QUE/DOX for 24 h through apoptosis detection kit. (G) The level of COX2 expression in RAW264.7 and B16F10 cells after treated with QUE at different concentrations *in vitro*. (H and I) The expression level of COX2 in Fig. 1G was analyzed by image J, RAW264.7 cells (H), B16F10 cells (I). Data are presented as mean ± SD, $n = 4$, **$P < 0.01$, ***$P < 0.001$, ****$P < 0.0001$ *vs.* indicated.

3.2. Synthesis and characterization of DPQ-DOX NPs

After confirming that QUE could improve the efficacy of DOX in a concentration dependent manner, we plan to graft QUE onto the carrier to increase the amount of QUE. The synthetic route of the pH/ROS dual-responsive prodrug polymer DEX-PBA-QUE is shown in Scheme 1. We carried out ^{1}H NMR spectrum (Supporting Information Fig. S1A and S1B) and infrared spectrum detection (Supporting Information Fig. S1C and S1D) to confirm the structure of the material. According to the calculation, the content of PBA in DEX-PBA is about 9.86% (*w/w*) and the content of QUE in DEX-PBA-QUE is 7.4% (*w/w*).
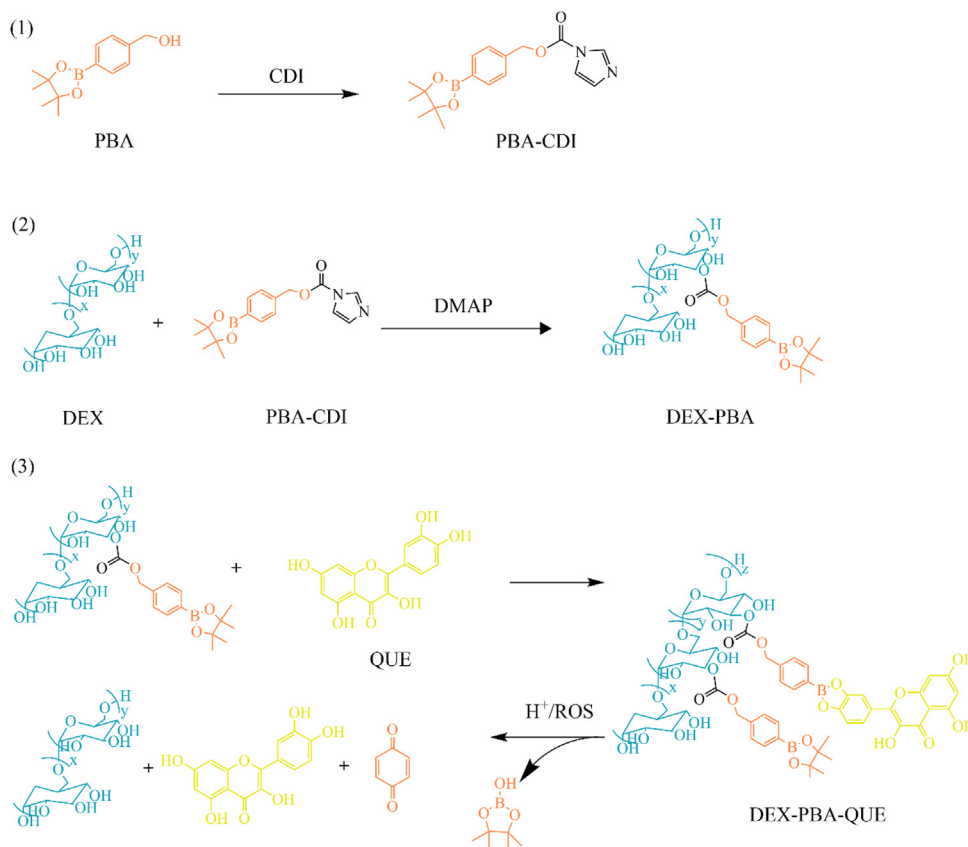
Scheme 1 The synthesis and degradation routes of DEX-PBA-QUE. The synthesis process involved the activation of PBA followed by grafting it onto DEX. Finally, QUE was grafted onto the compound *via* an ester bond to obtain DEX-PBA-QUE, which was degraded under weak acid or ROS-rich conditions as shown in the scheme.

The polymer material DEX-PBA-QUE was prepared into nanoparticles with a particle size of approximately 100 nm by self-assembly. To test the responsiveness of the material, referring to the method of Kyle E. Broaders[39], we measured the absorbance of the nanoparticles at various times and in different dispersion medium to analyze the degradation of the nanoparticles. In Fig. 2A, there was almost no change in the control group within 6 h, indicating that the nanoparticles were stable in PBS. While the degradation rate of nanoparticles in the pH 6.5 PBS group was up to 50% at 4 h. At 5 h, 90% of the nanoparticles in the peroxide group were degraded, and more than 90% of the nanoparticles in the pH 6.5 PBS plus H_2O_2 group underwent degradation at 2 h, and it could be observed that the nanoparticles in this group were almost transparent solution. These results indicate that the nanoparticles are quite stable under physiological conditions, but can be rapidly and responsively degraded in a weakly acid tumor environment containing ROS. The DEX-PBA-QUE has good acidic and ROS responsiveness. We have successfully prepared a dual-responsive material with a high grafting rate of QUE.

Then, we prepared DPQ-DOX NPs by encapsulating DOX in DEX-PBA-QUE. The size of the nanoparticles was 167.1 ± 2.92 nm, the polydispersity coefficient (PDI) was 0.1–0.2, and the zeta potential was −18.83 ± 2.84 mv as measured by Malvern Laser Particle Sizer (Fig. 2B and C). The nanoparticles showed relatively high encapsulation efficiency of both drugs. Considering the CI index and synergistic effect, the ratio of DOX/QUE (*w/w*) was chosen as 1:1 for the further researches[53−55].

Therefore, approximately same amount of DOX and QUE (around 7.4%) was loaded in the nanoparticles. The morphology of the nanoparticles was regularly spherical (Fig. 2D) as shown by the TEM. The changes of the size and PDI of the nanoparticles were measured in 10% serum or PBS at 37 °C and PBS at 25 °C to verify the stability of the nanoparticles *in vitro* and *in vivo*, and the results (Fig. 2E and F, Fig. S2) showed that the size and PDI of the nanoparticles didn't change significantly and tended to be stable, indicating the good stability of the nanoparticles. In addition, the morphological changes of the nanoparticles in different dispersion media were observed by TEM (Fig. 2G−I), and the nanoparticles degraded from regular spherical shape to irregular dotted or filamentary fragments under the action of acidic or reactive oxygen species, which further directly demonstrated that DPQ-DOX NPs also possessed the dual responsiveness of DPQ-DOX NPs.

3.3. Evaluation of dual responsive release behavior of drugs from nanoparticles

In vitro release assays were performed to measure the release characteristics of the drug in different release medium (Fig. 3A). As the results showed that free DOX was released completely and rapidly within a few h, while the nanoparticles in pH7.4 PBS were stable with almost no release in the first few h and no sudden release. The release of DPQ-DOX NPs increased slightly under weakly acidic conditions, with a final release of about 37%, while the final cumulative release rate was about 80% in the presence of
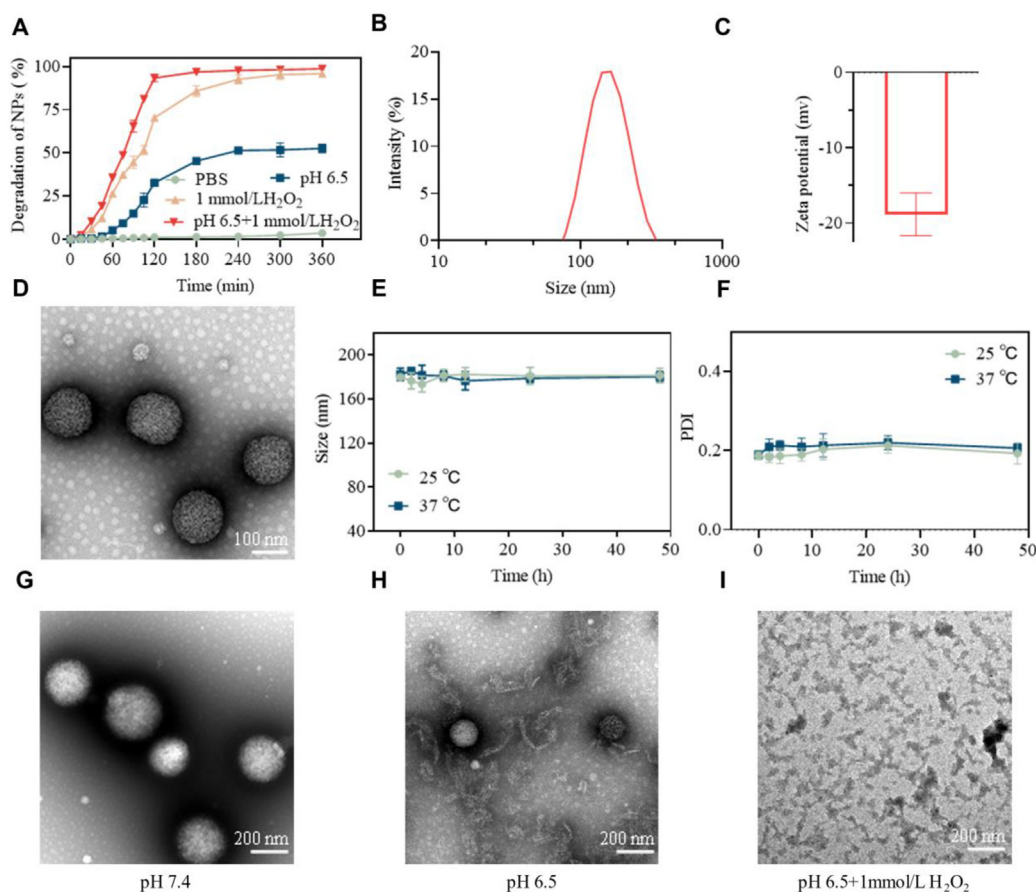
Figure 2 Characterization of DPQ-DOX NPs. (A) Degradation curves of DPQ NPs in pH7.4 PBS, pH 6.5 PBS, pH 7.4 PBS with 1 mmol/L H_2O_2 and pH 6.5 PBS with 1 mmol/L H_2O_2. (B) Size distribution graph of DPQ-DOX NPs. (C) Zeta potential distribution of DPQ-DOX NPs. (D) A representative TEM image of DPQ-DOX NPs. (E) and (F) The particle size and PDI variation of DPQ-DOX NPs after 48 h incubation in 50 % fetal bovine serum at different temperatures. (G−I) TEM of nanoparticles degradation in pH 6.5 or 1 mmol/L H_2O_2 after 12 h. Data are presented as mean ± SD, $n = 3$.

ROS. Under the superposition of acidity and H_2O_2, the cumulative release reached more than 60% within 8 h. The nanoparticle group had the fastest release rate, with a total release of about 95%, which was close to the free drug. These results demonstrated that nanoparticles can precisely release drugs in the weakly acidic and ROS-rich microenvironment, supporting the *in vivo* experiments.

3.4.   Cellular uptake experiments of nanoparticles

The PBA in DPQ-DOX NPs can specifically bind to SA highly expressed on the tumor surface to achieve tumor targeting. This effect can still occur in the weakly acidic TME[43,56]. However, SA is also expressed in erythrocytes, normal liver and lung[57]. In addition, the PBA may bind to many sugars under normal physiological conditions[58]. Therefore, it is easy to get off-target effects if the PBA is not closed. The tumor targeting effect can be improved by QUE blocking the PBA to avoid off-targeting. We verified the *in vitro* targeting of the nanoparticles by cellular uptake experiments[58−60]. To verify whether the grafting of QUE affects the targeting of PBA to tumors, we selected the pregrafting material DEX-PBA, prepared as nanoparticles DEX-PBA nanoparticles (DP NPs), as a control group. Qualitative analysis of cellular uptake revealed that the uptake of the preparation groups was higher than of free DOX, probably due to the

targeting effect of PBA (Fig. 3B). There was no significant difference between DPQ-DOX NPs and DP-DOX NPs. Quantitative analysis by flow cytometry (Fig. 3C) showed the same results, with the uptake of DPQ-DOX NPs and DP-DOX NPs being 1.5 and 1.8 times higher than that of free DOX, respectively. To make the results more direct and accurate, we also measured the intracellular DOX content after repeated freeze-thaw lysis of the cells (Fig. 3D), and the uptake fraction of DPQ-DOX NPs was 2.2 times that of free DOX and 1.3 times that of the control. Furthermore, the binding of PBA to SA was verified by competition inhibition of uptake assay. As shown in Fig. 3D and E, the uptake of nanoparticles by B16F10 cells in the APBA/SA incubation-treated group was significantly lower than the PBS group. The incorporation of free APBA/SA directly interfered with the interaction of PBA in nanoparticles with SA on the cell surface. It indicated the tumor-targeting effect of PBA in DPQ-DOX NPs.

The addition of QUE didn't decrease drug uptake, instead there was a slight increase. It is possible that the high concentration of glucose in the medium interfered with the binding of PBA to SA. The DPQ-DOX NPs avoided the interference due to the confinement effect of QUE, which favored the competitive binding of SA. This anti-off-target effect is negligible *in vitro* and should be more significant during *in vivo* targeting experiments. In addition,
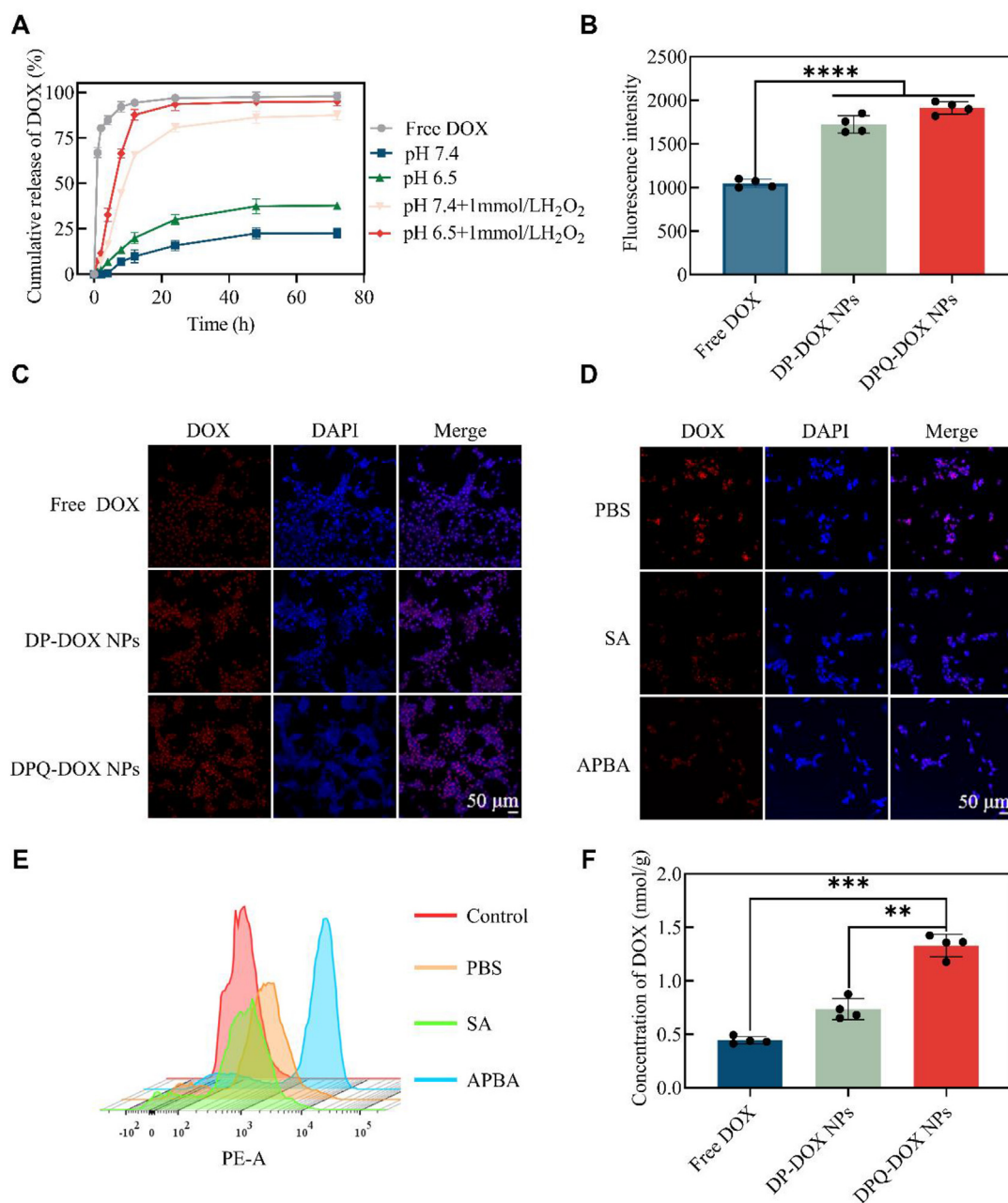
Figure 3 Release behavior and cellular uptake of DPQ-DOX NPs. (A) Release behavior of DOX from DPQ-DOX NPs after treatment with various release buffers. (B) Quantification of DOX uptake by B16F10 cells from different formulations by flow cytometry. (C) Cellular uptake of DOX from different formulations on B16F10 cells imaged qualitatively by CLSM. (D–E) The uptake of DOX by B16F10 cells in competitive inhibition assay was determined by CLSM and flow cytometry. (F) Quantification of DOX uptake by B16F10 cells from different formulations by LC–MS/MS. Data are presented as mean $\pm$ SD, $n = 4$, $**P < 0.01$, $***P < 0.00$, $****P < 0.0001$ vs. indicated.

multidrug resistance (MDR) in cancer cells is also a major problem[55]. MDR is mainly caused by the overexpression of P-gp with drug pump function[61]. Studies have shown that when chemotherapeutic drugs are combined with QUE, QUE can inhibit the expression of P-gp and improve the accumulation of drugs in cells, which could reverse the MDR effect[62,63]. Based on the regulatory effect of QUE on the efflux transporter (such as P-gp, BCRP, MRP1)[61,64], we hypothesized that the uptake of modified nanoparticles would be higher than that of the control group, which may also be related to the facilitating effect of QUE itself on cellular uptake. In conclusion, compared to free DOX, DPQ-

DOX NPs increased drug accumulation in tumor s and achieved its tumor targeting effect in vitro.

3.5. In vivo distribution of DPQ-DOX NPs

Systemic toxicity and poor drug accumulation frequently constrain the efficacy of chemotherapy. The adequate tumor accumulation is an important factor for improving chemotherapy. The tumor targeting effect of DPQ NPs was further verified by in vivo distribution experiments. The distribution results showed that all the drugs gradually accumulated at the tumor site after

administration. The accumulation reached a maximum level at 8 h and decreased thereafter. DPQ-DiD NPs showed more targeted accumulation at the tumor with a 5.95-fold increase in fluorescence intensity compared to free DiD and a 1.65-fold increase compared to DP-DiD NPs at 8 h (Fig. 4A and B). This result was consistent with the cellular uptake study. Similar results were observed in isolated tumor mice sections at 8 h post-administration where DiD distribution was examined by CLSM (Fig. 4E).

In order to more intuitively investigate the distribution of DOX in the body, LC−MS/MS was used to further examine the distribution of DOX in tumors and major organs. It was found that DPQ-DOX NPs had the highest DOX concentration in tumors (Fig. 4C and E). Among them, the accumulation at the tumor site still remained the highest at 8 h (Fig. 4C). At this time, the nanoparticle group of drugs was most abundant in the liver, while free DOX was less abundant. This is a relatively normal phenomenon, due to the nature of nanoparticles such as particle size. It is worth noting that nanoparticles reduced renal and heart distribution. Compared to DP-DOX NPs, DPQ-DOX NPs significantly reduced drug accumulation in the liver and lung (Fig. 4D). This is consistent with our earlier discussion that QUE enclosed PBA avoiding off-target effects. The role of reducing off-targeting to improve the effect of targeting tumors is more pronounced *in vivo*. The experimental results showed that DPQ-DOX NPs improved the distribution of chemotherapy drugs *in vivo*, significantly increased the accumulation of drugs in tumor sites, and realized the targeting effect of drugs on tumors, which is expected to improve the efficacy of drugs. In addition, the pharmacokinetics of DPQ-DOX NPs were also explored and the plasma concentrations of DOX were evaluated by LC-MS/MS. Just as the Supporting Information Fig. S3 and Table S1 showed, loading the DOX into nanoparticles can improve the bioavailability of DOX. And there is no difference between the nanoparticle groups.

3.6.   *In vitro drug efficacy experiments of nanoparticles*

To evaluate the actual anti-tumor efficacy of the prepared drug delivery system, the *in vitro* cytotoxicity of DPQ-DOX NPs on B16F10 cells was first determined by MTT (Fig. 5A−E). Not surprisingly, free DOX had the lowest IC_{50} in the drug alone group due to its non-release process and transient entry into the cells. Consistent with previous studies, free QUE had no direct cytotoxicity at low concentrations, and the cytotoxicity was significantly enhanced after combination of DOX and QUE. It is worth noting that the cytotoxicity of the free drug was not affected by the changes in pH and H_2O_2 conditions. In contrast, DP-DOX NPs and DPQ-DOX NPs were less cytotoxic in pH 7.4 PBS due to the lack of responsive release conditions resulting in less drug release. In fact, both groups of nanoparticles showed increased cytotoxicity in the presence of H_2O_2. More importantly, in the pH 6.5 + 1 mmol/L H_2O_2 group, the IC_{50} of DPQ-DOX NPs decreased to 0.5 times that of free DOX, 0.87 times that of free QUE plus DOX (Supporting Information Table S2), owing to its rapid responsive release in TME. Similarly, the cell apoptosis experiment manifested that the highest rate of apoptosis was induced by DPQ-DOX NPs in B16F10 cells under weak acid and reactive oxygen conditions compared to free drug and other conditions, which increased to 67%, yet only 37.8% for DOX alone (Fig. 5F and G). These results suggested that DPQ-DOX NPs exhibited greater cytotoxicity than free drug, possibly because of its targeted and responsive release. Using QUE as a

prodrug not only greatly improved the properties of QUE, but it also realized co-administration with DOX, which could produce a synergistic effect of QUE and DOX to enhance tumor efficacy.

3.7.   *In vivo efficacy of DPQ-DOX NPs in mice*

Encouraged by the *in vitro* efficacy assay, we used the same animal model as the *in vivo* biodistribution assay to evaluate the *in vivo* anti-tumor efficiency of the designed drug delivery system. On the 11th day after intravenous injection, tumor-bearing B16F10 mice treated with different drugs were euthanized and tumor size was measured before and after execution. The separated tumors were further analyzed and studied. The change curves of tumor volume (Fig. 6C), tumor weight (Fig. 6D) and tumor inhibition rate (Fig. 6E) showed that DPQ-DOX NPs had the best anti-tumor effect with 90.5 ± 3.1% tumor inhibition rate compared to the saline group, while the inhibition rates of DPQ NPs, DOX and DP-DOX NPs were 16.13%, 43.75% and 65.28%, respectively. In addition, Kaplan-Meier survival curves showed that DPQ-DOX NPs significantly prolonged the survival of mice, with a median survival of 42 days compared with 24 days in the saline group (Fig. 6F and Supporting Information Table S3). These figures demonstrated that the high drug loading of the QUE and DOX co-loaded responsive release system enhanced the overall treatment effectiveness in melanoma.

Paraffin sections of isolated tumors were subjected to H&E staining, immunofluorescence TUNEL staining and immunohistochemical Ki67 assay. H&E staining (Fig. 6I) displayed that all tumor tissues exhibited some degree of necrosis, but the DPQ-DOX NPs group had the highest percentage of necrosis and the best treatment effect. This was verified in subsequent experiments. The cell necrosis in the physiological saline group this was due to excessive tumor growth causing ischemia and hypoxia and spontaneous tumor death. The fluorescence images detected by TUNEL (Fig. 6G) showed that the saline group had the lowest percentage of apoptotic cells (2.04%), while the DPQ-DOX NPs group had the highest percentage of apoptotic cells (91.87%). In the immunohistological experiments, the proliferation marker Ki-67 was stained. Consistent with the H&E analysis, the control group had the greatest level of proliferation with a ratio of the number of Ki-67 positive cells (yellow) to the total number of cells (blue) of 48.13%, while the DPQ-DOX NPs group was lower (1.04%). All these results together showed that the DPQ-DOX NPs group was significant in treating tumors *in vivo*. We hypothesized that this favorable anti-tumor effect may be related to the fact that the delivery system improved certain mechanisms of drug action *in vivo*.

3.8.   *DPQ-DOX NPs enhance the chemoimmunotherapy effect by remodeling the tumor microenvironment via COX2-PGE2 axis*

The immunomodulatory effect was analyzed to further explore the mechanisms underlying the anti-tumor efficacy of DPQ-DOX NPs. For a more comprehensive comparison of efficacy, free QUE group, free QUE-DOX combination group (a small amount of DMSO dissolved, subcutaneous injection), and DEX-PBA combined load DOX and QUE (DP-DOX + QUE NPs) group were added, which had a low QUE load, and the deficiency was supplemented by subcutaneous injection. As can be seen, the DPQ-DOX NPs group still had the best anti-tumor effect in all groups (Supporting Information Fig. S5).
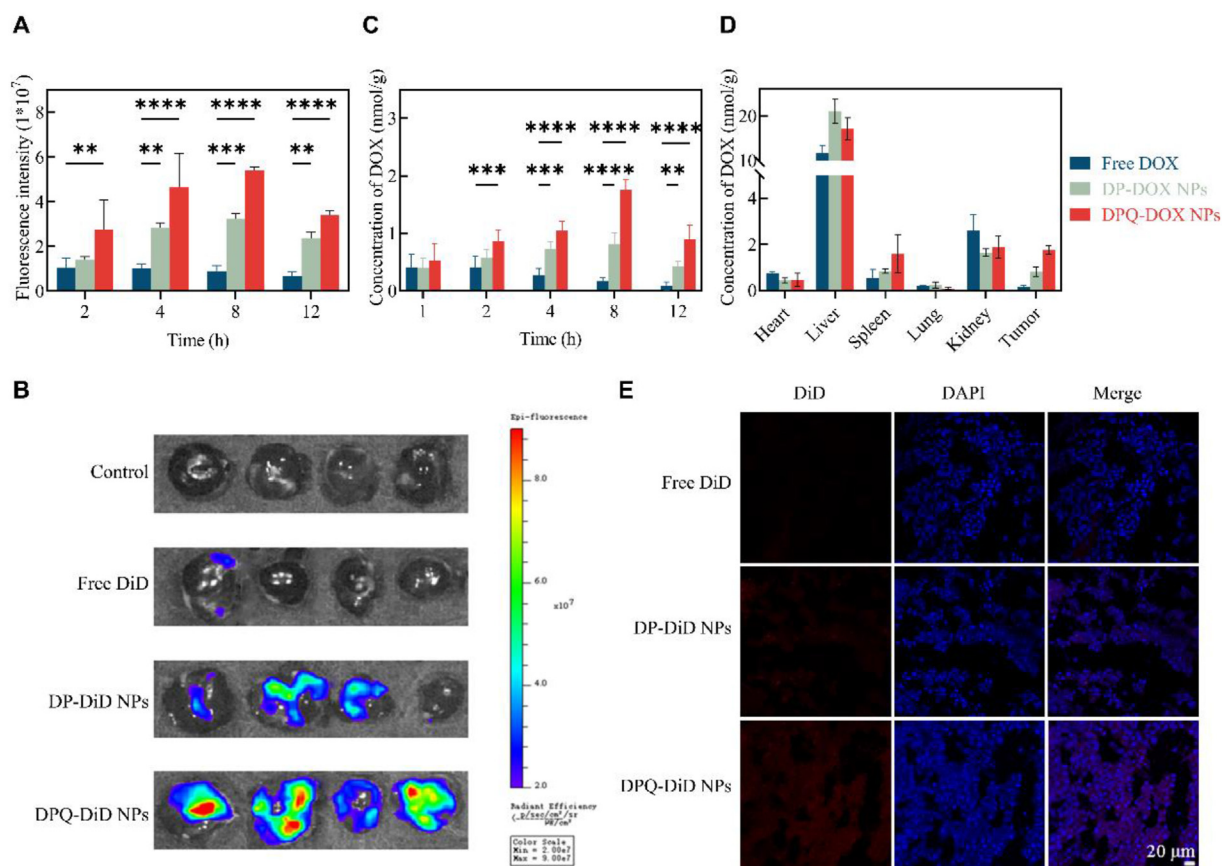
Figure 4 The *in vivo* distribution of DPQ NPs. (A) Semi-quantification of tumor fluorescence in B16F10 tumor-bearing mice injected with different DiD preparations at various time points. (B) The *ex vivo* fluorescence images of tumors executed at 8 h after injection of different DiD preparations in B16F10 tumor-bearing mice. (C) LC−MS/MS determination of DOX levels in tumors at 1, 2, 4, 8 and 12 h after different treatments. (D) LC−MS/MS determination of *in vivo* DOX levels in each organ at 8 h after different treatments. (E) Fluorescence images of tumor-bearing mice treated with different DiD preparations for 8 h observed by CLSM. Data are presented as mean $\pm$ SD, $n = 4$, **$P < 0.01$, ***$P < 0.00$, ****$P < 0.0001$ *vs*. indicated.

DOX is a typical inducer of ICD that relies on the coordinated expression and release of a series of injury-related pattern molecules, typically chemotherapeutic agents that promote exocytosis from the endoplasmic reticulum (ER) and increase adenosine triphosphate (ATP) secretion and HMGB1 release, and these molecules can stimulate DCs maturation and further activation of T cells[65,66]. We first determined whether DPQ-DOX NPs successfully induced ICD *in vivo* by immunofluorescence and immunohistochemical examination of tumor tissue. The results confirmed that DOX promoted CRT exposure and HMGB1 release, while the effect was better when combined with QUE, especially the DPQ-DOX NPs group had the highest exposure. It is possible that the promoting effect of QUE on DOX cytotoxicity increased the exposure of DAMPs. These results suggested that the combination of DOX and QUE loaded nanoparticles can significantly enhance the tumor immunogenicity based on tumor ICD (Fig. 7A).

Then the flow cytometry was used to analyze the infiltration of lymphocytes in mice. DCs are an important class of antigen-presenting cells, and whether antigen can reach and be taken up by DCs and induce their maturation is crucial for the subsequent immune response. We first measured the expression levels of three surface molecules, including CD40, CD80 and CD86, on the surface of DCs in draining lymph nodes, and DPQ-DOX NPs possessed the strongest ability to induce DCs maturation with the proportion of CD40⁺CD80⁺DC increasing from $23.1 \pm 4.14\%$ to $71.73 \pm 3.17\%$, and the proportion of CD80⁺CD86⁺DC increasing from $24.3 \pm 1.93\%$ to $68.28 \pm 2.71\%$ compared with the control (Fig. 7B−E). In addition, CD103⁺DC can promote intratumoral CTLs infiltration and anti-tumor immunity by stimulating CTLs[67,68]. Compared to the other groups, the frequency of CD103⁺DC was significantly increased in the DPQ-DOX NPs treated group (Fig. 7F). Thus, most of the DCs in the mice have been activated, and the mature DCs can deliver tumor-associated antigens to the immune site and further stimulate the generation of tumor-specific CTLs (CD8⁺ T cells), which can directly kill tumor cells, and helper T lymphocytes (Th, CD4⁺ T cell). The level of activated T cells in each group was detected. According to the measurement results (Fig. 7H−J), the proportion of CTLs (CD3⁺CD8⁺ T cells) and Th cells (CD3⁺CD4⁺ T cells) in DPQ-DOX NPs group was the highest, demonstrating that the tumor immune system was successfully activated. Specifically, the proportion of CD3⁺CD8⁺ T cells increased from $18.88 \pm 1.12\%$ to $48.95 \pm 2.42\%$ in the DPQ-DOX NPs group, which was 2.66 times higher than that in the PBS group, showing that the tumor immune system was effectively activated. Meanwhile, NK cells
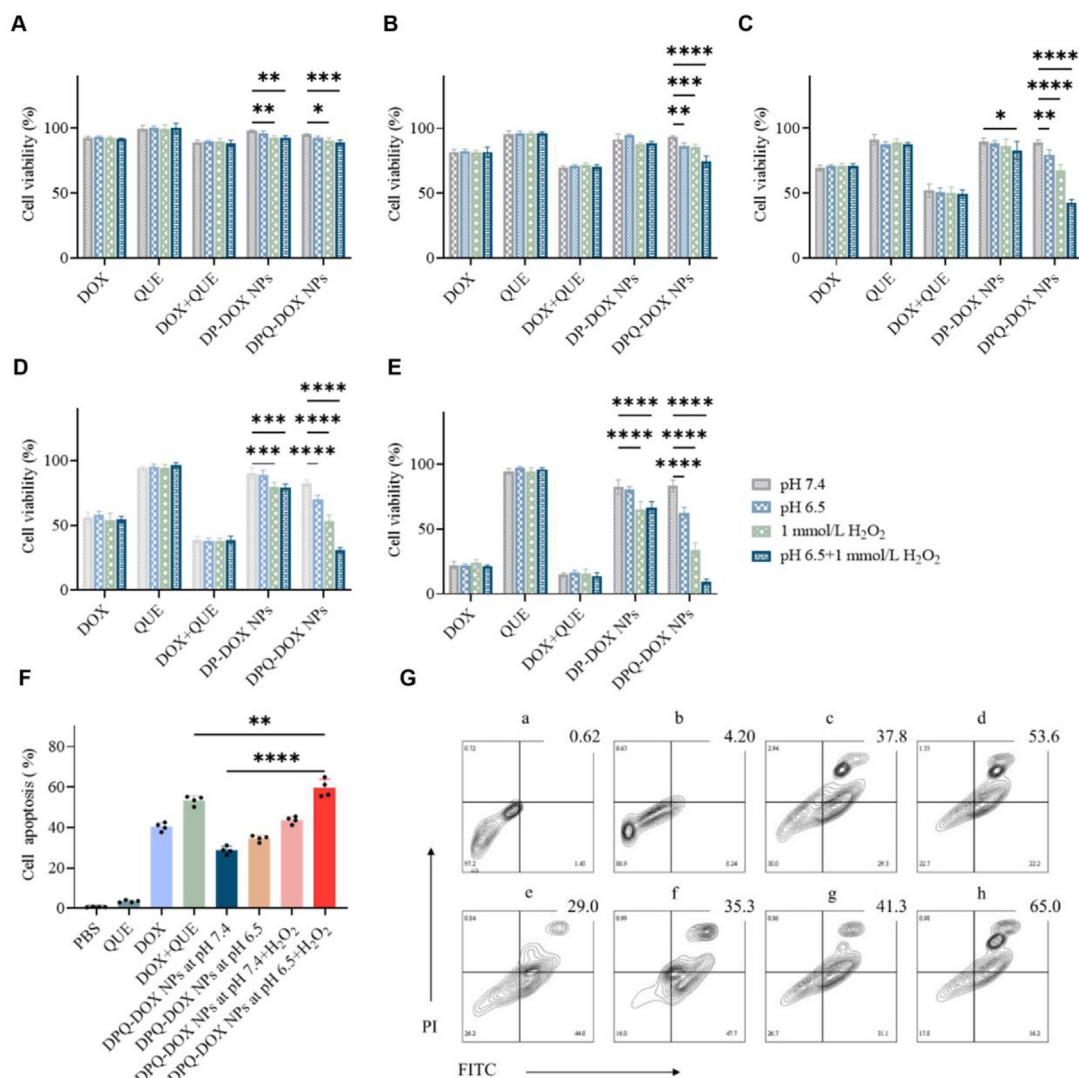
Figure 5 *In vitro* anti-tumor effect of DPQ-DOX NPs. (A−E) The cytotoxic effect of different preparations at different concentrations on B16F10 cells was evaluated, the concentration of DOX: (A) 156 ng/mL, (B) 312 ng/mL, (C) 625 ng/mL, (D) 1250 ng/mL, (E) 2500 ng/mL. (F) The relative percentages of early apoptosis cells. (G) Flow cytometry analysis of apoptotic and necrotic B16F10 cells induced by various formulations for 24 h *via* apoptosis detection kit. (a) PBS, (b) QUE, (c) DOX, (d) DOX + QUE, (e) DPQ-DOX NPs at pH 7.4, (f) DPQ-DOX NPs at pH 6.5, (g) DPQ-DOX NPs at 1 mmol/L H_2O_2, (h) DPQ-DOX NPs at pH 6.5 + 1 mmol/L H_2O_2. Data are presented as mean ± SD, $n = 4$, $*P < 0.05$, $**P < 0.01$, $***P < 0.00$, $****P < 0.0001$ *vs.* indicated.

gradually increased in the drug combination group, with the maximum percentage in the DPQ-DOX NPs group being 4.76 ± 0.87% (Fig. 7G).

Moreover, the ability of DPQ-DOX NPs to promote DCs maturation was also investigated *in vitro*. BMDCs were extracted from healthy male C57 mice, and the supernatants of tumor cells culture medium treated with different preparations for 24 h were co-incubated with DCs for 24 h. After stimulation of the group with LPS as a positive control, the positive rate of DC cell surface molecules (CD80, CD86, CD40) was detected by flow cytometry, and the results are shown in Fig. 8G−I. The untreated tumor supernatants could not promote the upregulation of CD86, CD40, CD80, and the free QUE-treated group also did not cause a notable increase in surface molecules, indicating that these influencing factors could not effectively induce the maturation of DCs. Under the effect of DOX and DOX + QUE, DP-DOX NPs, DPQ-DOX NPs, the surface molecules (CD86, CD40, CD80) of

DCs were upregulated at different levels. More importantly, the DPQ-DOX NPs group induced the highest expression of both double positive CD86, CD40, CD80, demonstrating its ability to maximally stimulate the maturation of DCs.

In the previous study, we found that QUE could affect the COX2-PGE$_2$ axis. The COX2/PGE$_2$ axis promoted tumor immune escape by hindering DCs recruitment and increasing immunosuppressive components. Therefore, we hypothesized that DPQ-DOX NPs could enhance the immunotherapeutic effect by affecting the COX2-PGE$_2$ pathway. Firstly, the expression levels of the COX2-PGE$_2$ axis were measured in tumor tissues, and in line with what we have earlier demonstrated, QUE reduced the expression of COX2. Notably, the combination with DOX suppressed the tumor induced upregulation of COX2. The DPQ-DOX NPs group showed the best suppression with a relative expression level of COX2 of 0.49, which was about 1/3 of that of the DP-DOX NPs group (Fig. 8A−C). The expression of COX2 showed
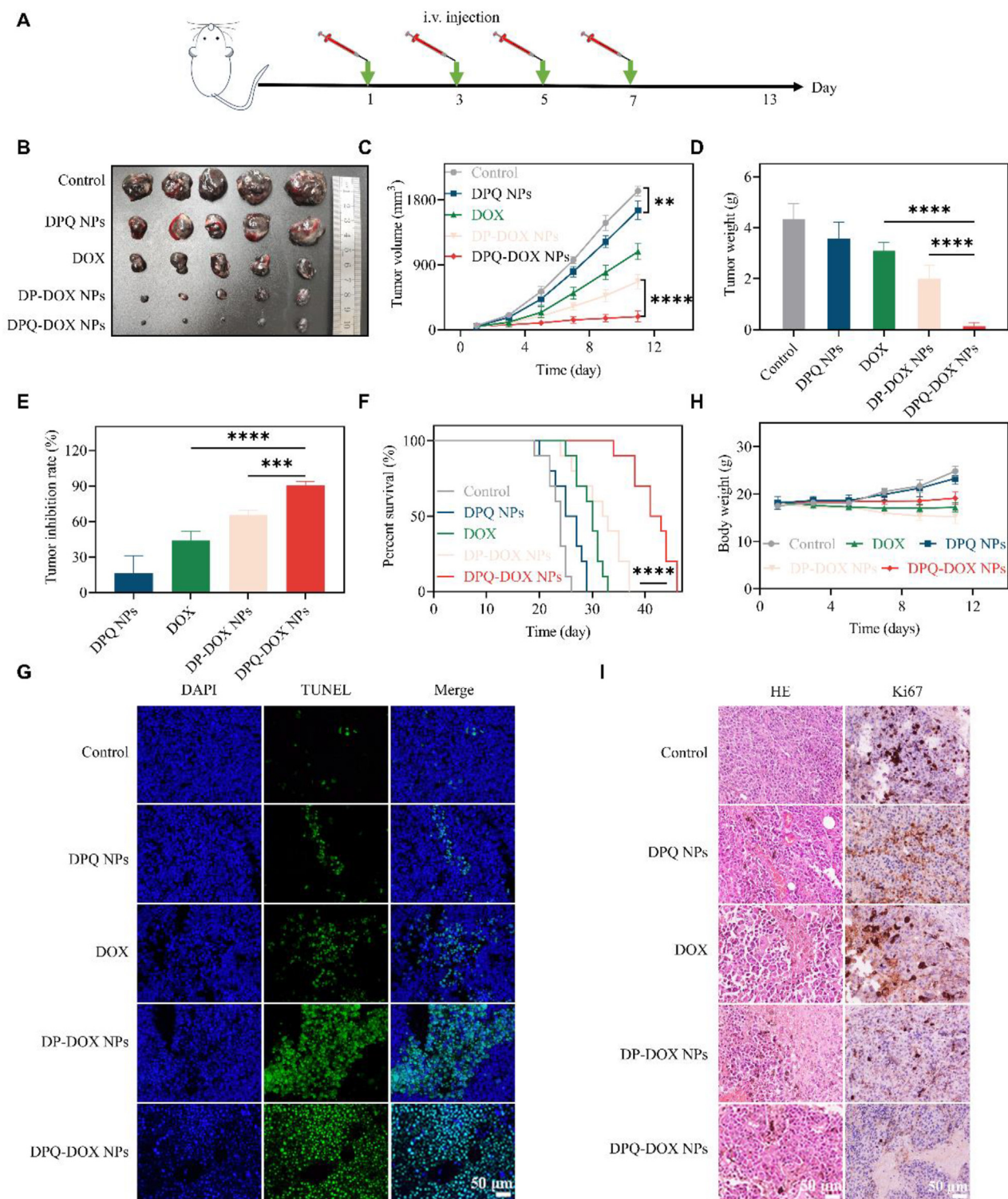
Figure 6 *In vivo* anti-tumor efficacy of DPQ-DOX NPs. (A) Illustration of the animal administration regimen. (B) Image of the B16F10 xenograft tumor at the end of therapy. (C) Tumor growth graphs of tumor-bearing mice after treatment with differing formulations. (D) Isolated tumor weight and tumor suppression rate. (E) Tumor inhibition rate in each group after different treatment. (F) Survival curves of B16F10 tumor-bearing mice in each group. (G) Representative fluorescence microscopy images of tumor tissues of TUNEL staining. (H) Body weight change curves of tumor-bearing mice during treatment. (I) H&E staining and Ki-67 staining of tumor tissues after treatment. Data are presented as mean $\pm$ SD, $n = 5$, **$P < 0.01$, ***$P < 0.00$, ****$P < 0.0001$ *vs*. indicated.
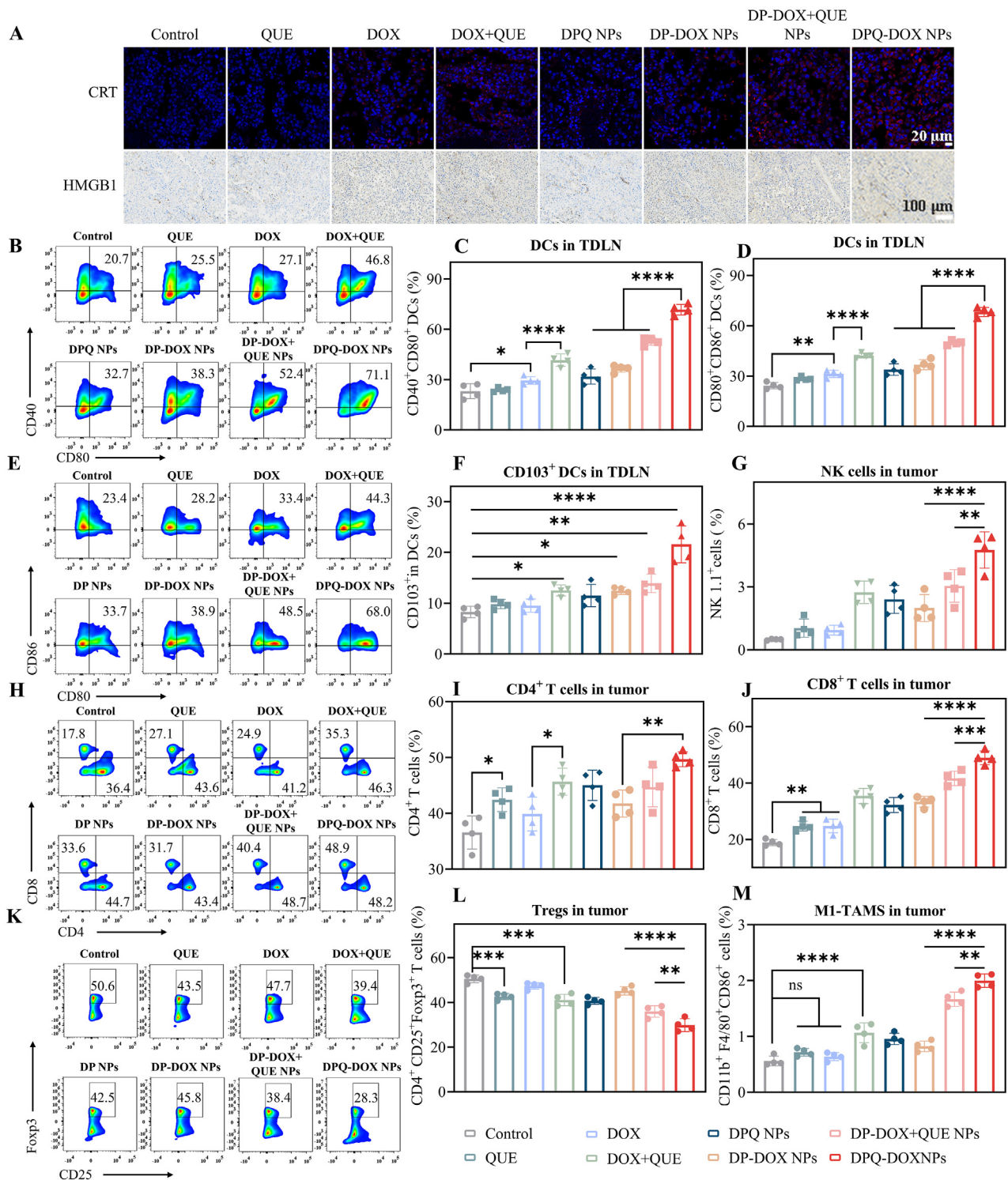
Figure 7 *In vivo* anti-tumor immune effect of DPQ-DOX NPs. (A) (A) The expression of calreticulin (CRT) and HMGB1 in B16F10 tumor tissues after treatment. (B), (E), (H) and (K) Representative FCM profiles of various immune effector cell, (B) and (E) mature DC cells; (H) CD8$^+$T cells (K)Tregs. (C), (D), (F), (G), (I) and (J) Quantitative data analysis of various immune cells, (C) and (D) matured DCs; (F) CD103$^+$DCs; (G) NK cells; (I) and (J) CD4$^+$, CD8$^+$T cells; (L) Tregs; (M) M1-tumo-associated macrophages (TAMS). Data are presented as mean ± SD, $n = 4$; *$P < 0.05$, **$P < 0.01$, ***$P < 0.00$, ****$P < 0.0001$ *vs.* indicated.
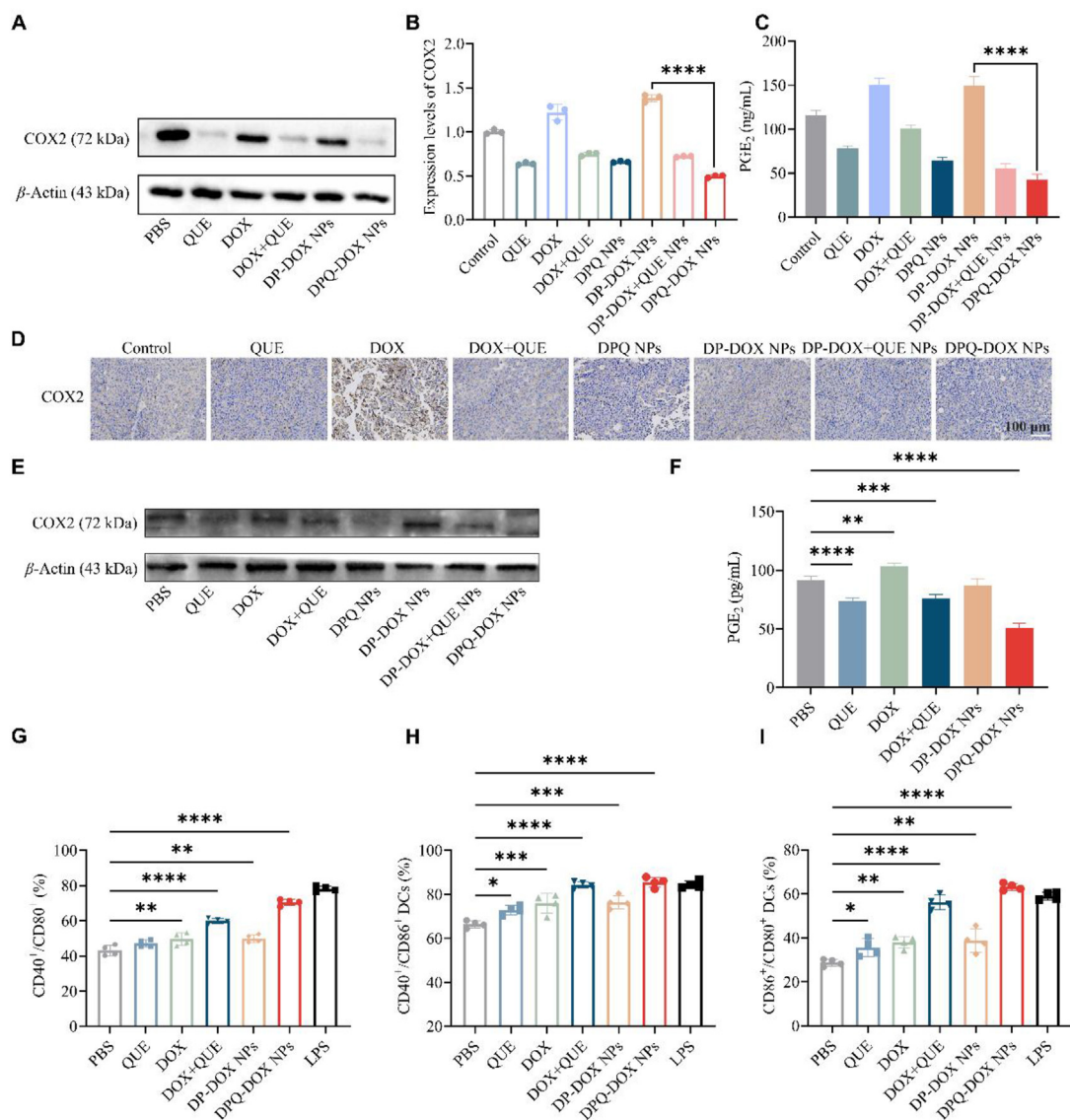
Figure 8 Effect of DPQ-DOX NPs on COX2-PGE$_2$ axis. (A–D) Analysis of COX2 and PGE$_2$ expression at the tumor site. (E) Expression levels of COX2 protein in B16F10 cells after treatment in different ways. (F) PGE$_2$ expression levels in B16F10 cell supernatants after treatment with different agents. (G–I) Determination of the effect of tumor cell supernatants on primary DCs maturation after treatment with different agents: (G) CD40$^+$CD80$^+$ DCs; (H) CD40$^+$CD86$^+$DCs; (I) CD80$^+$CD86$^+$ DCs. Data are presented as mean $\pm$ SD, $n = 4$; *$P < 0.05$, **$P < 0.01$, ***$P < 0.00$, ****$P < 0.0001$ $vs.$ indicated.

the same trend in the tumor staining results (Fig. 8D). We also evaluated whether the DPQ-DOX NPs could regulate COX2 expression levels in B16F10 cells. Western blotting was conducted to determine the expression level of COX2 in B16F10 cells after treatment with different preparations (Fig. 8E). It can be seen that QUE could effectively inhibit the expression of COX2 and the expression of COX2 is the lowest in the DPQ-DOX NPs group. Next, the levels of the metabolite PGE$_2$ downstream of COX2 were examined (Fig. 8F). Consistently, DOX in combination with QUE significantly reduced PGE$_2$ expression, and DPQ-DOX NPs had the best inhibitory effect.

As mentioned above, PGE$_2$ can act on a variety of cells and be involved in tumor immunomodulation. Having confirming the downregulation of the COX2-PGE$_2$ axis by nanoparticles, we examined their effect on tumor immunosuppression. Consequently, we examined the ratio of Tregs in tumor tissues. The Treg

ratio in the QUE group was $42.63 \pm 1.4\%$, which was 0.84 of that in the saline group, showing that QUE could reduce Tregs. The DPQ-DOX NPs group had the lowest percentage of Tregs (CD4$^+$Foxp3$^+$CD25$^+$) (Fig. 7K and L), which decreased from $50.58 \pm 1.69\%$ to $29.83 \pm 2.88\%$. In addition, other immunosuppressive cells at the tumor site were measured, such as myeloid suppressor cells (MDSCs, CD11b$^+$Gr-1$^+$) and M2 macrophages (CD11b$^+$CD206$^+$). In the DPQ-DOX NPs group, the proportions of MDSCs and M2 macrophages were decreased (Supporting Information Fig. S6), while immune-promoting M1 macrophages were increased (Fig. 7M). These results indicated that the DPQ-DOX NPs can significantly weaken tumor immune suppression compared with free drug alone. Therefore, after investigating the effect of DPQ-DOX NPs on the representative immune cells and the COX2-PGE$_2$ axis. We found that DOX increased immunogenicity and promoted the maturation of DCs through the

ICD. QUE down-regulated the expression of COX2, which in turn reduced the secretion of PGE2. The PGE$_2$ affected on a wide range of cells and was involved in the regulation of the TME. Overall, the DPQ-DOX NPs achieved synergistic enhancement of anti-tumor effects by remodeling the tumor immune environment *via* the COX2-PGE$_2$ axis.

We also examined the expression of P-gp, which is correlated with drug resistance. Notably, the DPQ-DOX NPs group had the lowest expression (Supporting Inforamtion Fig. S7A). Thus, the nanoparticles reduced tumor resistance to drugs and increased drug uptake, in line with the previously mentioned hypotheses. In addition, the COX2-PGE2 axis can regulate CCR7, which is associated with tumor metastasis. We evaluated the expression of CCR7 and showed that the nanoparticle could inhibit the over-expression of CCR7 (Fig. S7B). This suggested that the DPQ-DOX NPs delivery system may also play a role in inhibiting tumor metastasis.

3.9. Safety study

We evaluated the safety of the drug delivery system. Body mass index in mice is a pivotal marker of systemic toxicity and side effects. It can be seen that mice in the saline and blank nanoparticle groups slightly gained weight due to tumor growth (Fig. 6H), mice in the free DOX and DP-DOX NPs lost weight due to DOX toxicity, and the weight curve of mice in the DPQ-DOX NPs group was largely stable over time, indicating low systemic toxicity of the prepared nanoparticles. The H&E stained images of the major tissues (Supporting Information Fig. S8) showed diffuse tumor metastasis in the lung tissue of the saline group, cardiotoxicity in the free DOX group with marked thinning of myocardial muscle fibres, most of which lysed and broke, and some nephrotoxicity, hepatotoxicity with mild oedema seen in the liver cells, marked reduction in glomerular volume, partial glomerulosclerosis, reduced white marrow percentage in the spleen, lymphatic damage, and possible immunosuppressive effects were also seen in the DP-DOX NPs group, but to a minor extent, while no metastases were seen in the DPQ-DOX NPs group, with mild myocardial lysis, and the rest of the organs were normal with no obvious abnormal histopathology. We next measured the changes in the numbers of WBC, RBC and PLT in the blood at the end of treatment. We could see that the WBC, RBC and PLT in the free DOX and DP-DOX NPs groups were reduced, probably due to the myelosuppressive effect of DOX, while the levels were increased in the DPQ-DOX NPs group (Supporting Information Fig. S9A−S9C), indicating that DPQ-DOX NPs can effectively slow down the myelosuppressive response of DOX and reduce the toxic side effects. The results of serum biochemical assays were consistent with H&E staining, and free DOX had some organ toxicity (Fig. S9D−S9F), LDH, CK levels in response to the cardiotoxicity of free DOX were alleviated in the nanoparticle group. In the DPQ-DOX NPs group, other liver function and renal function parameters were also close to those of the control group, indicating that the drug delivery system reduced toxicity and had a good safety profile.

4. Conclusions

In summary, we developed a pH/ROS dual-responsive targeted drug delivery system for improved anti-tumor chemoimmunotherapy. The DPQ-DOX NPs precisely targeted to the tumor site and responsively released DOX and QUE. Subsequently, the delivery system enhanced tumor immunogenicity by stimulating ICD with DOX and affected a variety of immune cells by regulating the COX2-PGE2 axis through QUE. This synergistic effect increased mature DCs, Th cells and CTLs at the tumor site, decreased the proportion of Tregs and promoted macrophage polarization from M2 to M1, thereby remodeling the immune microenvironment. The strategy significantly increased QUE loading and enhanced chemoimmunotherapy compared to conventional nano-delivery systems, inhibited tumor growth and prolonged survival in mice, which may contribute to the development of more effective chemoimmunotherapy delivery systems. It may also be effective in improving tumor resistance and metastasis.

Author contributions

Leilei Wang designed the research, carried out the experiments, analyzed the data, and wrote the original manuscript. Shanshan He analyzed the data and edited the original manuscript. Rong Liu and Yuan Xue performed experiments and analyzed the data. Yuan Quan, Rongying Shi and Xueying Yang participated part of the experiments. Qing Lin and Xun Sun provided resources and project administration for experiments. Zhirong Zhang provided funding and supervised the project. Ling Zhang provided funding and revised the manuscript. All of the authors have read and approved the final manuscript.

Conflicts of interest

The authors declare no conflicts of interest.

Appendix A.   Supporting information

Supporting data to this article can be found online at https://doi.org/10.1016/j.apsb.2023.12.001.

References

1. Siegel RL, Miller KD, Fuchs HE, Jemal A. Cancer statistics, 2021. *Ca - Cancer J Clin* 2021;**71**:7−33.
2. Dagenais GR, Leong DP, Rangarajan S, Lanas F, Lopez-Jaramillo P, Gupta R, et al. Variations in common diseases, hospital admissions, and deaths in middle-aged adults in 21 countries from five continents (PURE): a prospective cohort study. *Lancet* 2020;**395**:785−94.
3. Chen Q, Ke H, Dai Z, Liu Z. Nanoscale theranostics for physical stimulus-responsive cancer therapies. *Biomaterials* 2015;**73**:214−30.
4. Debela DT, Muzazu SGY, Heraro KD, Ndalama MT, Mesele BW, Haile DC, et al. New approaches and procedures for cancer treatment: current perspectives. *SAGE Open Med* 2021;205031212110343.
5. Arruebo M, Vilaboa N, Saez-Gutierrez B, Lambea J, Tres A, Valladares M, et al. Assessment of the evolution of cancer treatment therapies. *Cancers* 2011;**3**:3279−330.
6. Behranvand N, Nasri F, Zolfaghari Emameh R, Khani P, Hosseini A, Garssen J, et al. Chemotherapy: a double-edged sword in cancer treatment. *Cancer Immunol Immunother* 2021;**71**:507−26.

7. Khan H, Mirzaei HR, Amiri A, Kupeli Akkol E, Ashhad Halimi SM, Mirzaei H. Glyco-nanoparticles: new drug delivery systems in cancer therapy. *Semin Cancer Biol* 2021;**69**:24−42.

8. Dawson MA, Kouzarides T. Cancer epigenetics: from mechanism to therapy. *Cell* 2012;**150**:12−27.

9. Czarnecka AM, Bartnik E, Fiedorowicz M, Rutkowski P. Targeted therapy in melanoma and mechanisms of resistance. *Int J Mol Sci* 2020;**21**:119250.

10. Meng QY, Cong HL, Hu H, Xu FJ. Rational design and latest advances of codelivery systems for cancer therapy. *Materials Today Bio* 2020;**7**: 100056.

11. Al Bostami RD, Abuwatfa WH, Husseini GA. Recent advances in nanoparticle-based co-delivery systems for cancer therapy. *Nanomaterials* 2022;**12**:2672.

12. Guo P, He Y, Xu T, Pi C, Jiang Q, Wei Y, et al. Co-delivery system of chemotherapy drugs and active ingredients from natural plants: a brief overview of preclinical research for cancer treatment. *Expet Opin Drug Deliv* 2020;**17**:665−75.

13. Gao Q, Feng J, Liu W, Wen C, Wu Y, Liao Q, et al. Opportunities and challenges for co-delivery nanomedicines based on combination of phytochemicals with chemotherapeutic drugs in cancer treatment. *Adv Drug Deliv Rev* 2022;**188**:114445.

14. Rauf A, Imran M, Khan IA, Ur-Rehman M, Gilani SA, Mehmood Z, et al. Anticancer potential of quercetin: a comprehensive review. *Phytother Res* 2018;**32**:2109−30.

15. Li B, Shao H, Gao L, Li H, Sheng H, Zhu L. Nano-drug co-delivery system of natural active ingredients and chemotherapy drugs for cancer treatment: a review. *Drug Deliv* 2022;**29**:2130−61.

16. Sun D, Zou Y, Song L, Han S, Yang H, Chu D, et al. A cyclodextrin-based nanoformulation achieves co-delivery of ginsenoside Rg3 and quercetin for chemo-immunotherapy in colorectal cancer. *Acta Pharm Sin B* 2022;**12**:378−93.

17. Ezzati M, Yousefi B, Velaei K, Safa A. A review on anti-cancer properties of Quercetin in breast cancer. *Life Sci* 2020;**248**:117463.

18. Murakami A, Ashida H, Terao J. Multitargeted cancer prevention by quercetin. *Cancer Lett* 2008;**269**:315−25.

19. Tang SM, Deng XT, Zhou J, Li QP, Ge XX, Miao L. Pharmacological basis and new insights of quercetin action in respect to its anti-cancer effects. *Biomed Pharmacother* 2020;**121**:109604.

20. Asgharian P, Tazekand AP, Hosseini K, Forouhandeh H, Ghasemnejad T, Ranjbar M, et al. Potential mechanisms of quercetin in cancer prevention: focus on cellular and molecular targets. *Cancer Cell Int* 2022;**22**:257.

21. Wang Y, Yu H, Wang S, Gai C, Cui X, Xu Z, et al. Targeted delivery of quercetin by nanoparticles based on chitosan sensitizing paclitaxel-resistant lung cancer cells to paclitaxel. *Mater Sci Eng C* 2021;**119**: 111442.

22. Pham TND, Stempel S, Shields MA, Spaulding C, Kumar K, Bentrem DJ, et al. Quercetin enhances the anti-tumor effects of BET inhibitors by suppressing hnRNPA1. *Int J Mol Sci* 2019;**20**:4293.

23. Sun J-H, Liang X, Cai M, Yan L, Chen Z, Guo L, et al. Protein-crowned micelles for targeted and synergistic tumor-associated macrophage reprogramming to enhance cancer treatment. *Nano Lett* 2022;**22**:4410−20.

24. Take Y, Koizumi S, Nagahisa A. Prostaglandin E receptor 4 antagonist in cancer immunotherapy: mechanisms of action. *Front Immunol* 2020;**11**:324.

25. Thumkeo D, Punyawatthananukool S, Prasongtanakij S, Matsuura R, Arima K, Nie H, et al. PGE2-EP2/EP4 signaling elicits immunosuppression by driving the mregDC-Treg axis in inflammatory tumor microenvironment. *Cell Rep* 2022;**39**:110914.

26. Finetti F, Travelli C, Ercoli J, Colombo G, Buoso E, Trabalzini L. Prostaglandin E2 and cancer: insight into tumor progression and immunity. *Biology* 2020;**9**:434.

27. Ramyaa P, krishnaswamy R, Padma VV. Quercetin modulates OTA-induced oxidative stress and redox signalling in HepG2 cells—up regulation of Nrf2 expression and down regulation of NF-κB and COX-2. *Biochim Biophys Acta Gen Subj* 2014;**1840**:681−92.

28. Tao Q, Xiao X, Shi D, Liu L, Wang J, Xie X, et al. Quercetin suppresses cyclooxygenase-2 expression and angiogenesis through inactivation of p300 signaling. *PLoS One* 2011;**6**:e22934.

29. Yu Z, Guo J, Hu M, Gao Y, Huang L. Icaritin exacerbates mitophagy and synergizes with doxorubicin to induce immunogenic cell death in hepatocellular carcinoma. *ACS Nano* 2020;**14**:4816−28.

30. Han S, Bi S, Guo T, Sun D, Zou Y, Wang L, et al. Nano co-delivery of Plumbagin and Dihydrotanshinone I reverses immunosuppressive TME of liver cancer. *J Control Release* 2022;**348**:250−63.

31. Zhao J, Huang H, Zhao J, Xiong X, Zheng S, Wei X, et al. A hybrid bacterium with tumor-associated macrophage polarization for enhanced photothermal-immunotherapy. *Acta Pharm Sin B* 2022;**12**:2683−94.

32. Guo J, Zou Y, Huang L. Nano delivery of chemotherapeutic ICD Inducers for tumor immunotherapy. *Small Methods* 2023;**7**:e2201307.

33. Hu M, Huang L. Strategies targeting tumor immune and stromal microenvironment and their clinical relevance. *Adv Drug Deliv Rev* 2022;**183**:114137.

34. Qureshi WA, Zhao R, Wang H, Ji T, Ding Y, Ihsan A, et al. Co-delivery of doxorubicin and quercetin *via* mPEG−PLGA copolymer assembly for synergistic anti-tumor efficacy and reducing cardiotoxicity. *Sci Bull* 2016;**61**:1689−98.

35. Zhang J, Luo Y, Zhao X, Li X, Li K, Chen D, et al. Co-delivery of doxorubicin and the traditional Chinese medicine quercetin using biotin−PEG2000−DSPE modified liposomes for the treatment of multidrug resistant breast cancer. *RSC Adv* 2016;**6**:113173−84.

36. Ma T, Liu Y, Wu Q, Luo L, Cui Y, Wang X, et al. Quercetin-modified metal-organic frameworks for dual sensitization of radiotherapy in tumor tissues by inhibiting the carbonic anhydrase IX. *ACS Nano* 2019;**13**:4209−19.

37. Xu D, Hu MJ, Wang YQ, Cui YL. Antioxidant activities of quercetin and its complexes for medicinal application. *Molecules* 2019;**24**:1123.

38. Stockert JC, Blazquez-Castro A, Canete M, Horobin RW, Villanueva A. MTT assay for cell viability: intracellular localization of the formazan product is in lipid droplets. *Acta Histochem* 2012;**114**: 785−96.

39. Broaders KE, Grandhe S, Frechet JM. A biocompatible oxidation-triggered carrier polymer with potential in therapeutics. *J Am Chem Soc* 2011;**133**:756−8.

40. Elshaarani T, Yu H, Wang L, Lin L, Wang N, ur Rahman Naveed K, et al. Dextran-crosslinked glucose responsive nanogels with a self-regulated insulin release at physiological conditions. *Eur Polym J* 2020;**125**:109505.

41. Ghezzi M, Pescina S, Padula C, Santi P, Del Favero E, Cantù L, et al. Polymeric micelles in drug delivery: an insight of the techniques for their characterization and assessment in biorelevant conditions. *J Control Release* 2021;**332**:312−36.

42. Taha A, Ahmed E, Ismaiel A, Ashokkumar M, Xu X, Pan S, et al. Ultrasonic emulsification: an overview on the preparation of different emulsifiers-stabilized emulsions. *Trends Food Sci Technol* 2020;**105**: 363−77.

43. Long Y, Lu Z, Mei L, Li M, Ren K, Wang X, et al. Enhanced melanoma-targeted therapy by "Fru-Blocked" phenyboronic acid-modified multiphase antimetastatic micellar nanoparticles. *Adv Sci* 2018;**5**:1800229.

44. Sauter M, Sauter RJ, Nording H, Olbrich M, Emschermann F, Langer HF. Protocol to isolate and analyze mouse bone marrow derived dendritic cells (BMDC). *STAR Protocols* 2022;**3**:101664.

45. Erlich Z, Shlomovitz I, Edry-Botzer L, Cohen H, Frank D, Wang H, et al. Macrophages, rather than DCs, are responsible for inflammasome activity in the GM-CSF BMDC model. *Nat Immunol* 2019;**20**: 397−406.

46. Wang L, Ding K, Zheng C, Xiao H, Liu X, Sun L, et al. Detachable Nanoparticle-enhanced chemoimmunotherapy based on precise killing of tumor seeds and normalizing the growing soil strategy. *Nano Lett* 2020;**20**:6272−80.

47. Fu T, Dai LJ, Wu SY, Xiao Y, Ma D, Jiang YZ, et al. Spatial architecture of the immune microenvironment orchestrates tumor immunity and therapeutic response. *J Hematol Oncol* 2021;**14**:98.

48. Soriano AF, Helfrich BA, Chan DC, Heasley LE, Bunn PA, Chou TC. Synergistic effects of new chemopreventive agents and conventional cytotoxic agents against human lung cancer cell lines. *Cancer Res* 1999;**59 24**:6178−84.

49. Yan JJ, Du GH, Qin XM, Gao L. Baicalein attenuates the neuro-inflammation in LPS-activated BV-2 microglial cells through suppression of pro-inflammatory cytokines, COX2/NF-κB expressions and regulation of metabolic abnormality. *Int Immunopharm* 2020;**79**: 106092.

50. Wang J, Liu YT, Xiao L, Zhu L, Wang Q, Yan T. Anti-inflammatory effects of apigenin in lipopolysaccharide-induced inflammatory in acute lung injury by suppressing COX-2 and NF-κB pathway. *Inflammation* 2014;**37**:2085−90.

51. Kim JY, Park SJ, Yun KJ, Cho YW, Park HJ, Lee KT. Isoliquiritigenin isolated from the roots of Glycyrrhiza uralensis inhibits LPS-induced iNOS and COX-2 expression *via* the attenuation of NF-κB in RAW 264.7 macrophages. *Eur J Pharmacol* 2008;**584**:175−84.

52. Wang HM, Fu L, Cheng CC, Gao R, Lin MY, Su HL, et al. Inhibition of LPS-induced oxidative damages and potential anti-inflammatory effects of phyllanthus emblica extract *via* down-regulating NF-κB, COX-2, and iNOS in RAW 264.7 Cells. *Antioxidants* 2019;**8**:270.

53. Liu S, Guo Y, Huang R, Li J, Huang S, Kuang Y, et al. Gene and doxorubicin co-delivery system for targeting therapy of glioma. *Biomaterials* 2012;**33**:4907−16.

54. Fang J, Zhang S, Xue X, Zhu X, Song S, Wang B, et al. Quercetin and doxorubicin co-delivery using mesoporous silica nanoparticles enhance the efficacy of gastric carcinoma chemotherapy. *Int J Nanomed* 2018;**13**:5113−26.

55. Sun X, Li Y, Xu L, Shi X, Xu M, Tao X, et al. Heparin coated meta-organic framework co-delivering doxorubicin and quercetin for effective chemotherapy of lung carcinoma. *J Int Med Res* 2020;**48**: 300060519897185.

56. Fan B, Kang L, Chen L, Sun P, Jin M, Wang Q, et al. Systemic siRNA delivery with a dual pH-responsive and tumor-targeted nanovector for inhibiting tumor growth and spontaneous metastasis in orthotopic murine model of breast carcinoma. *Theranostics* 2017;**7**:357−76.

57. Deshayes S, Cabral H, Ishii T, Miura Y, Kobayashi S, Yamashita T, et al. Phenylboronic acid-installed polymeric micelles for targeting sialylated epitopes in solid tumors. *J Am Chem Soc* 2013;**135**: 15501−7.

58. Tang X, Sheng Q, Xu C, Li M, Rao J, Wang X, et al. pH/ATP cascade-responsive nano-courier with efficient tumor targeting and siRNA unloading for photothermal-immunotherapy. *Nano Today* 2021;**37**: 101083.

59. Huang Y, Zhang W, Xu Y, Zhu S, Wu Y, Chen T, et al. Dynamic core crosslinked camptothecin prodrug micelles with reduction sensitivity and boronic acid-mediated enhanced endocytosis: an intelligent tumor-targeted delivery nanoplatform. *Int J Pharm* 2020;**580**:119250.

60. Yang X, Gao S, Yang B, Yang Z, Lou F, Huang P, et al. Bioinspired tumorrosslinked camptothecin prodrug micelles with reduction sensitivity and boronic acid-mediated enhanced endocytosis: an inte. *Adv Sci* 2023;**10**:e2302272.

61. Dallavalle S, Dobričić V, Lazzarato L, Gazzano E, Machuqueiro M, Pajeva I, et al. Improvement of conventional anti-cancer drugs as new tools against multidrug resistant tumors. *Drug Resist Updates* 2020; **50**:100682.

62. Li S, Yuan S, Zhao Q, Wang B, Wang X, Li K. Quercetin enhances chemotherapeutic effect of doxorubicin against human breast cancer cells while reducing toxic side effects of it. *Biomed Pharmacother* 2018;**100**:441−7.

63. Li S, Zhao Q, Wang B, Yuan S, Wang X, Li K. Quercetin reversed MDR in breast cancer cells through down-regulating P-gp expression and eliminating cancer stem cells mediated by YB-1 nuclear translocation. *Phytother Res* 2018;**32**:1530−6.

64. Chen Z, Huang C, Ma T, Jiang L, Tang L, Shi T, et al. Reversal effect of quercetin on multidrug resistance *via* FZD7/β-catenin pathway in hepatocellular carcinoma cells. *Phytomedicine* 2018;**43**:37−45.

65. Chen S, Li D, Du X, He X, Huang M, Wang Y, et al. Carrier-free nanoassembly of doxorubicin prodrug and siRNA for combinationally inducing immunogenic cell death and reversing immunosuppression. *Nano Today* 2020;**35**:100924.

66. Kim M, Lee JS, Kim W, Lee JH, Jun BH, Kim KS, et al. Aptamer-conjugated nano-liposome for immunogenic chemotherapy with reversal of immunosuppression. *J Control Release* 2022;**348**:893−910.

67. Pfirschke C, Siwicki M, Liao HW, Pittet MJ. Tumor microenvironment: no effector T cells without dendritic cells. *Cancer Cell* 2017;**31**:614−5.

68. Barilla RM, Diskin B, Caso RC, Lee KB, Mohan N, Buttar C, et al. Specialized dendritic cells induce tumor-promoting IL-10^{+}IL-17^{+} FoxP3^{neg} regulatory CD4^{+} T cells in pancreatic carcinoma. *Nat Commun* 2019;**10**:1424.